UNIVERSITY OF OKLAHOMA

GRADUATE COLLEGE

DEVELOPMENT OF A VERIFIED NON-LINEAR WINKLER MODEL FOR THE SEISMIC ANALYSIS OF PILES IN IMPROVED GROUND

A THESIS

SUBMITTED TO THE CEES GRADUATE FACULTY

in partial fulfillment of the requirements for the

Degree of

MASTER OF SCIENCE

By

SUMANGALI SIVAKUMARAN

Norman, Oklahoma

2019

DEVELOPMENT OF A VERIFIED NON-LINEAR WINKLER MODEL FOR THE SEISMIC ANALYSIS OF PILES IN IMPROVED GROUND

A THESIS APPROVED FOR THE
SCHOOL OF CIVIL ENGINEERING AND ENVIRONMENTAL SCIENCE

BY THE COMMITTEE CONSISTING OF

Dr. Kanthasamy K. Muraleetharan, Chair

Dr. Amy B. Cerato

Dr. Philip S. Harvey

This thesis is dedicated

to my family.

Acknowledgements

I am very grateful to my advisor, Professor Muraleetharan for his guidance and intellectual support throughout my graduate studies and research work at the University of Oklahoma (OU). I am especially thankful to him for encouraging me while I pursued my interests in numerical modeling and computer programming. He encouraged me to present my research work at the Engineering Mechanics Institute Conference 2019 at Caltech which was a great opportunity for me. I want to thank Professors Cerato and Harvey for serving on my committee and providing their expertise and experience in the field of soil dynamics and earthquake engineering. I would also like to thank Professors Harvey and Muraleetharan for giving me a valuable opportunity to work with them in the Acceleration Bridge Construction - University Transportatiton Center (ABC-UTC) funded project.

Thank you for the geotechnical faculty of the School of Civil Engineering and Environmental Science at OU for your dedication in teaching and research work. I really enjoyed and learned a lot of new and interesting things from you while taking classes. I am grateful to all my classmates and friends in the Geotechnical Engineering Group at OU for all of their help and support. I will remember all the intellectual conversations and the social interactions with them forever.

A very special thanks to my family who supported me throughout my graduate studies. I am grateful to them for loving me, for motivating me, and for believing in me while I pursued my educational goals so far away from home.

Table of Contents

List of Tables

List of Figures

Abstract

Several ground improvement techniques that are proven to be effective and economical solutions to increase the lateral stiffness and strength of weak soils around piles often result in unwarranted conservative volumes of soil improvement. There are also no rigorous techniques to analyze seismic behavior of piles in improved soils that can be utilized in day-to-day engineering practice. In this study, a stand-alone finite element computer code called DYPAC (Dynamic Piles Analysis Code) using the Beams on Non-linear Winkler Foundation (BNWF) approach is developed. DYPAC analyzes the seismic response of a single pile in improved and unimproved soils. This computer code models the pile as a beam element and the non-linear soil behavior as springs and viscous dashpots using a non-linear *p-y* element, where *y* is the pile displacement and *p* is the soil reaction per unit length of the pile. This non-linear *p-y* element accounts for soil yielding, gapping, radiation damping, and soil cave-in and recompression during seismic loading simulations. A method to modify the *p-y* curves to account for limited lateral extent of ground improvement is proposed and validated. The input parameters for these curves can directly be obtained from in-situ or laboratory soil tests. These *p-y* curves were input in to DYPAC to analyze a series of dynamic centrifuge tests of single piles in soils improved using Cement Deep Soil Mixing (CDSM). Free-field site response analyses were performed using the DEEPSOIL computer program and the soil displacement-time histories were input to the free-field ends of the non-linear *p-y* elements. The predictions made by DYPAC are validated using the centrifuge test results.

CHAPTER 1: INTRODUCTION

1.1 Background

Deep pile foundations support civil engineering structures such as buildings, highway bridges, electric transmission towers, port wharves, off-shore oil production platforms, and wind turbines. Earthquakes have caused significant damage to civil engineering structures all over the world due to inadequate lateral load capacity and performance of piles foundations. The ocean waves, traffic, blast, and wind are some of the other sources of lateral loading on piles. When the piles are constructed on weak soils, the consequences of lateral loading intensifies the lateral displacements of piles and can lead to loss of structural integrity. Weak soils are soft clays and liquefiable loose sands and these are widespread in the US, in places such as Northern California, Southern Nevada, Washington, Eastern Missouri, and Arkansas.

The lateral load behavior of piles can be controlled by deploying a number of soil improvement techniques around piles such as surface compaction, chemical stabilization (e.g., CDSM and grouting), vibroflotation, drainage methods, and precompression and consolidation. These soil improvement techniques enhance the strength and stiffness of soils and limit the lateral movement and distresses in piles during lateral loading. These techniques have been proven to be effective and economical in practice to enhance the lateral stiffness and strength of weak soils in seismic regions compared to the traditional approach that increases the diameter and number of piles. Simple computer programs are available to analyze the pile foundation under static and cyclic loading, but not under seismic loading. Finite element computer codes based on fully coupled continuum models are complicated and time consuming and are therefore not convenient for day-to-day designs.

1.2 Motivation

Different soil improvement techniques are used in practice however, due to complex soil-structure interactions occurring during earthquakes, there is no rigorous method available to analyze and design the pile foundations in improved soils. The current state of practice is to analyze soil-structure interactions in improved soils using the computer codes developed to study cyclic, one- dimensional behavior of soil-pile interactions without any considerations for seismic loads or lateral extent of the improved soil. As a result, the ground improvement around piles often results in unwarranted conservative volumes of soil improvement leading to costly designs.

This study focuses on developing a stand-alone computer code to analyze seismic soil-pile interactions in improved and unimproved soils. A simple method is required to capture the lateral extent of ground improvement around piles. The effects of soil improvement dimensions on the seismic soil-structure interactions are to be investigated using the verified computer code. The key motivation is to distribute the simplified, user-friendly computer code to practicing engineers so that they may design pile foundations in improved soils more accurately. It is expected that the computer code with the proposed methodology will lead to safer and economical structures in earthquake prone areas.

1.3 Research Objectives

- Formulate the governing equations to model the seismic soil-structure interactions using the Beams on Non-linear Winkler Foundation (BNWF) approach
- Identify suitable dynamic *p-y* curves to model the behavior of soil-pile interactions during seismic loading

- Develop a numerical model to solve the governing equations
- Propose and validate a simple method to account for lateral extent of soil improvement around a single pile
- Validate the numerical model predictions using centrifuge test results.

1.4 Thesis Organization

Chapter 2 begins with the discussion of the Winkler models. Different static and dynamic *p-y* curves and their pros and cons are discussed in detail. This chapter proceeds with the derivation of the governing equations for seismic soil-structure interaction problems using BNWF approach. The finite element solution and the matrices involved are then discussed. Finally, a numerical scheme is developed based on the Hilber-Hughes-Taylor (HHT)-α method (Hilber et al., 1977) to solve the governing equations.

A method to characterize the laterally loaded piles surrounded by CDSM improved soft clay is proposed and validated in Chapeter 3. The *p-y* curves are modified based on the proposed method and incorporated into the LPILE (Ensoft Inc, 2016) computer porgram. The LPILE-predicted values are compared with a series of pseudo-static centrifuge test results.

The details of a computer code based on the numerical model presented in Chapter 2 are given in Chapter 4. The computer code predictions of the pile responses in improved and unimproved soils under seismic loading are then shown in this chapter and compared to a series of seismic centrifuge test results for validation purposes.

In Chapter 5 outcomes of this study are summarized, conclusions are derived, and recommendations for future research are presented.

CHAPTER 2: NUMERICAL MODELING OF SEISMIC SOIL-STRUCTURE INTERACTION USING A NON-LINEAR WINKLER MODEL

2.1 Previous Work on *p-y* Curves

Winkler (1867) developed a simplified method called Beams on Elastic Foundation that is commonly used in civil engineering practice today to analyze soil-pile interactions. This approach models the pile as a beam element and the soil as infinite number of discrete spring elements with the interactions described using a *p-y* curve. Here, "*p*" denotes lateral soil resistance per unit length of the pile, and "*y*" denotes the lateral pile displacement. Later, this concept was extended as the Beams on Non-linear Winkler Foundation (BNWF) using discrete non-linear springs (Figure 2.1) to account for non-linearity of soils. Full-scale field experiments or reduced-scale centrifuge tests were used to derive the *p-y* curves. The relationship between *p* and *y* is a function of soil depth, soil stress-strain properties, and the pile diameter. Based on full-scale field experiments, *p-y* curves were proposed by Matlock (1970) for soft clay, by Reese and Welch (1975) and Reese et al. (1975) for stiff clay, and by Reese et al. (1974) for sand.

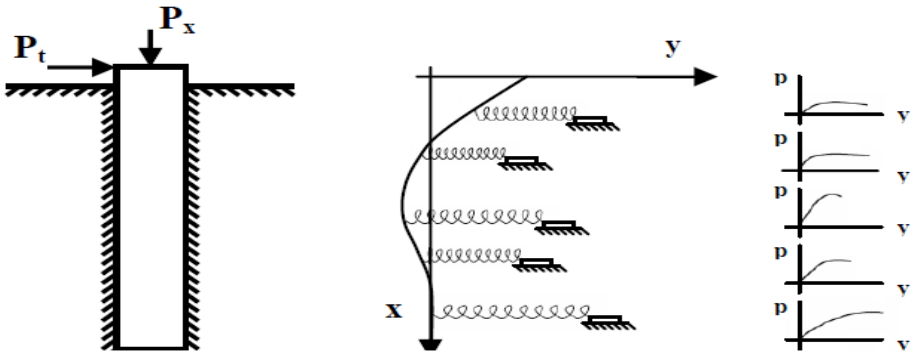

Figure 2.1 Discrete nonlinear springs along the pile to simulate soil-pile interactions (from Sritharan and Huang, 2010)

The BNWF models are simple, user-friendly, and an attractive approach in practice for many structural and geotechnical engineers to analyze soil-pile interactions under static or cyclic loading. The main advantage of BNWF is, with the limited computational effort, these models can satisfactorily account for soil non-linearity while still allowing for detailed structural modeling including structural non-linearities (Allotey and El Naggar, 2008a). The popular commercial finite difference computer program, LPILE, uses the BNWF approach and predicts the single pile responses satisfactorily under static and cyclic loading.

The main disadvantage of a BNWF model is the idealization of soil continuum as discrete, uncoupled springs (Allotey and El Naggar, 2008a; Soltani and Muraleetharan, 2018). Most BNWF models account for static and cyclic loading, not seismic loading on piles. These models possess limitations when applied to seismic loading conditions, such as, (a) inability to consider cycle-by-cycle soil-pile interactions, (b) inadequate modeling of kinematic interactions, and (c) ignoring inertial effects (Finn, 2005).

Past studies have developed dynamic BNWF models to simulate the lateral seismic soil-pile interactions, by accounting for the hysteretic interactions between soils and piles due to (a) opening and closing of gaps between soil and pile, (b) degradation of stiffness and strength of soil and pile, (c) loading, unloading and reloading behavior, (d) radiation damping of pile, and (e) pile and superstructure inertial effects (Boulanger et al., 1999; Gerolymos and Gazetas, 2005a; Allotey and El Naggar, 2008a; Soltani and Muraleetharan, 2018).

Boulanger et al. (1999) developed a non-linear *p-y* element that includes elastic, plastic, and gap components (Figure 2.2) that are connected in series. The elastic component simulates the far-field motion of the soil using a linear spring and a dashpot in parallel to model radiation

damping. The plastic component simulates the near field motion of the soil adjacent to the pile using a non-linear spring that considers the degradation of stiffness and strength. The gap component simulates the drag force on the pile when it moves within the gap by using a non-linear drag spring. The transition from the gap to contact was made smooth by a parallel non-linear closure spring. The gap formation is represented by a flat section with a small soil resistance in the *p-y* curve (Figure 2.3). The resulting seismic *p-y* curve for soft clay (Figure 2.3a), qualitatively replicated the experimental curve from lateral cyclic load test conducted by Matlock (1970) as shown in Figure 2.3b.

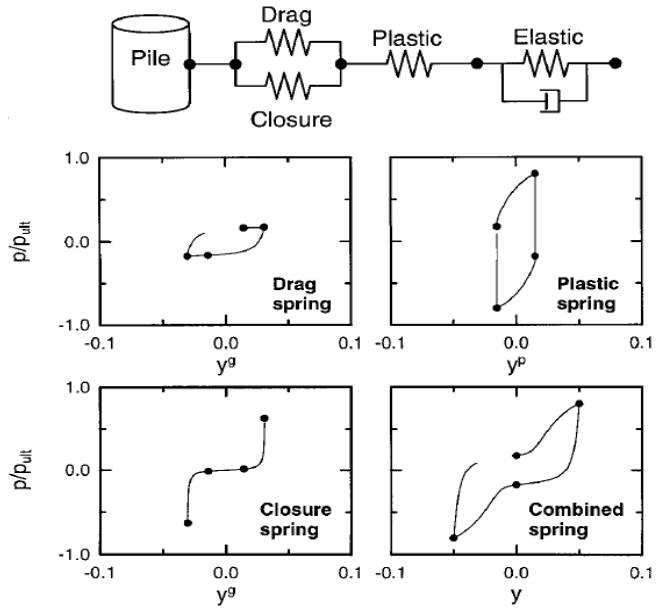

Figure 2.2 Nonlinear *p-y* element that includes elastic, plastic, and gap components (from Boulanger et al., 1999)

Allotey and El Naggar (2008a) developed a versatile, multi-linear, numerical model for the BNWF for both shallow and deep foundations, considering the effects of loading and unloading, gapping, strength and stiffness degradation, and radiation damping. A companion study, based on the developed numerical model, showed that the effect of soil cave-in and

recompression due to lateral cyclic response of soil–pile systems, decreases the pile maximum moment and moves its point of occurrence closer to the ground surface, and increases hysteretic energy dissipation (Allotey and El Naggar, 2008b).

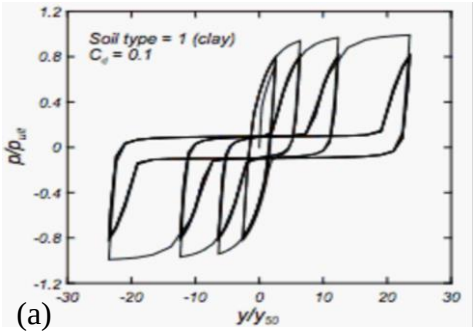

(a)

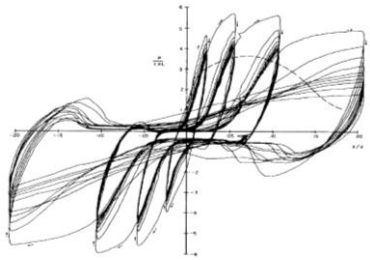

(b)

Figure 2.3 Dynamic *p-y* curves for soft clay (a) using Boulanger et al. (1999) model (from Mazzoni et al., 2006) (b) obtained from Matlock's (1970) centrifuge test

The basic Bouc-Wen model that was initially developed by Bouc (1967) and then extended by Wen (1976) consists of hysteretic springs and viscous dashpots placed in parallel, and it contains a first-order non-linear differential equation to predict the restoring force to a given relative displacement. The original model did not consider the strength and stiffness degradation and gapping when relating the restoring force to a given relative displacement. Many researchers came up with extended Bouc-Wen models to incorporate strength and stiffness degradation and gap formation to solve structural related, gapping problems in wood, steel, and concrete structures, and structural health monitoring problems (Baber and Noori, 1985; Loh and Chung, 1993; Sengupta and Li, 2013; Kottari et al., 2014; Pelliciari et al., 2018). Later, a few studies adapted and extended Basic Bouc-Wen model to simulate the *p-y* curves for seismic soil-structure interaction problems (Gerolymos and Gazetas, 2006; Soneji and Jangid, 2008; Soltani and Muraleetharan, 2018).

Gerolymos and Gazetas (2005a) adapted and extended the Bouc-Wen model and

developed a constitutive model called 'BWGG' model, by including an interaction spring and dashpot connected in parallel. The 'BWGG' model captured the effects of yielding, separation, radiation damping, degradation, and pore water pressure generation. This model was validated in a companion study, using in-situ static and seismic pile load tests results, and the predictions from the three-dimensional finite element analyses (Gerolymos and Gazetas, 2005b).

Soltani and Muraleetharan (2018) formulated a *p-y* element by adapting an Extended Bouc-Wen (EBW) model using a hysteresis spring and viscous dashpot connected in parallel. The model was calibrated to simulate the soil reaction on the pile at two different depths and it was able to replicate gapping, and strength and stiffness degradation between soil and pile. The main drawback of this model is the complicated method involved in identifying the EBW model parameters. Full-scale or reduced-scale test results are required to relate the soil properties such as Young's modulus and undrained shear strength to the EBW model parameters. This calibrating procedure turns out to be time- and labor-intensive and less attractive to practicing engineers.

2.2 Derivation of the Governing Equation for a Dynamic Beam

Hetenyi (1946) originally presented the derivation of the differential equation for a static beam on an elastic foundation. Here, the beam was subjected to a vertical axial load and lateral soil resistance. These governing equations are solved in the computer program, LPILE using a finite difference approach.

In this study, a beam on a non-linear Winkler foundation is considered (Figure 2.4) under dynamic loading. It is desirable to incorporate the axial loading to consider P-Δ effects. In the

following derivations, the total pile displacement (y_{tot}) is a sum of base displacement (u_g) and the pile displacement relative to the base (y_{rp}). The soil displacement relative to the base is denoted by y_{rs}. The time histories of y_{rs} is an input to this analysis and are typically obtained by performing a site response analysis of the free-field far from the pile.

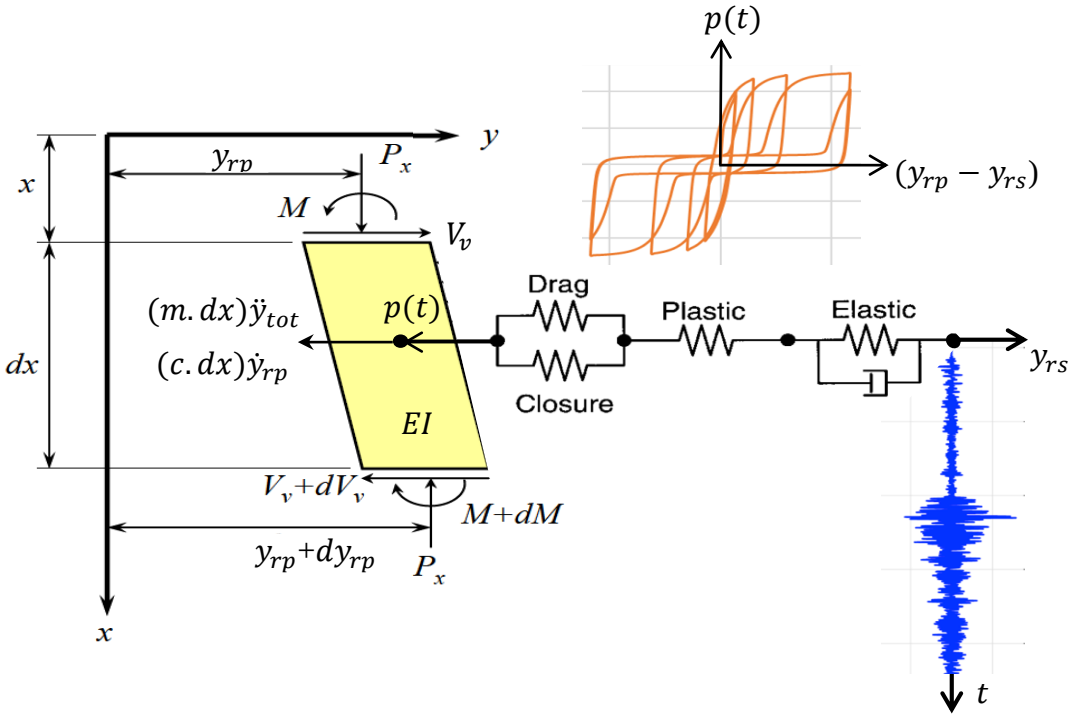

Figure 2.4 An infinitely small element from a dynamic beam

The equilibrium of moments (ignoring second-order terms) leads to the equation,

$$(M + dM) - M + P_x dy_{rp} - V_v dx = 0 \tag{2.1}$$

Rearranging Equation 2.1 leads to the following equation,

$$\frac{dM}{dx} + P_x \frac{dy_{rp}}{dx} - V_v = 0 \tag{2.2}$$

By differentiating Equation 2.2 with respect to *x*, the following equation is obtained

$$\frac{d^2M}{dx^2} + P_x \frac{d^2y_{rp}}{dx^2} - \frac{dV_v}{dx} = 0 \tag{2.3}$$

where the following relationship is noted (assuming EI is constant),

$$\frac{d^2M}{dx^2} = EI \frac{d^4y_{rp}}{dx^4} \tag{2.4}$$

The horizontal equilibrium of forces leads to the following equation:

$$(V_v + dV_v) - V_v + (m.dx)\frac{d^2y_{tot}}{dt^2} + (c.dx)\frac{dy_{rp}}{dt} + p(t)dx = 0 \tag{2.5}$$

Rearranging Equation 2.5 leads to the following equation,

$$\frac{dV_v}{dx} + m\frac{d^2y_{tot}}{dt^2} + c\frac{dy_{rp}}{dt} + p(t) = 0 \tag{2.6}$$

and substituting Equations 2.3 and 2.4 into Equation 2.6 will result in,

$$m\frac{d^2y_{tot}}{dt^2} + c\frac{dy_{rp}}{dt} + \{P_x\frac{d^2y_{rp}}{dx^2} + EI\frac{d^4y_{rp}}{dx^4}\} + p(t) = 0 \tag{2.7}$$

where:

$$\frac{d^2y_{tot}}{dt^2} = \frac{d^2u_g}{dt^2} + \frac{d^2y_{rp}}{dt^2} \tag{2.8}$$

Based on Winkler foundation approach, the lateral soil resistance per unit length ($p(t)$) can be related to pile diameter (b), soil subgrade modulus (K_T), and relative pile displacement $\left(y_{rp} - y_{rs}\right)$ via the following relation

$$p(t) = bK_T\left(y_{rp} - y_{rs}\right) \tag{2.9}$$

and substituting the Equations 2.8 and 2.9 into Equation 2.7 will result in

$$m\frac{d^2y_{rp}}{dt^2} + c\frac{dy_{rp}}{dt} + \{P_x\frac{d^2y_{rp}}{dx^2} + EI\frac{d^4y_{rp}}{dx^4}\} + bK_T\left(y_{rp} - y_{rs}\right) = -m\frac{d^2u_g}{dt^2} \quad (2.10)$$

where:

m = mass per unit length,

c = damping coefficient per unit length,

P_x = axial thrust load in the pile, and

EI = flexural rigidity.

The spatially discrete non-linear governing equation (Equation 2.10) for a dynamic soil-structure element can be given in matrix form as in the following equation:

$$[m_e]\ddot{y}_{rp} + [c_e]\dot{y}_{rp} + [k_e]y_{rp} + b[K_T]\left(y_{rp} - y_{rs}\right) = -[m_e]\ddot{u}_g \quad (2.11)$$

where $[m_e], [c_e]$, and $[k_e]$ are element mass, damping, and pile stiffness matrices, respectively; and $[K_T]$ denotes the tangent stiffness matrix of the *p-y* curve. The effect of axial load is neglected in this equation, assuming lateral displacements are small and P-Δ effect can be neglected.

The global equations for a dynamic soil-structure system can be given as

$$\mathbf{M}a + \mathbf{C}v + \mathbf{K_P}d + \mathbf{P} = \text{-}\mathbf{M}\ddot{u}_g \quad (2.12)$$

$$\mathbf{P} = b\mathbf{K_T}(d - u) \quad (2.13)$$

where $\mathbf{M}$, $\mathbf{C}$, and $\mathbf{K_P}$ are global mass, damping, and pile stiffness matrices, respectively. $\mathbf{P}$ is a soil resistance vector. a, v and d denote relative pile acceleration, velocity and displacement vectors, respectively, u and $\ddot{u}_g$ denote relative soil displacement and base motion vectors, respectively.

The various matrices in Equations 2.11 and 2.12 are given in the Appendix of this chapter. Matrices follow the order of the degrees of freedom shown in Figure 2.5.

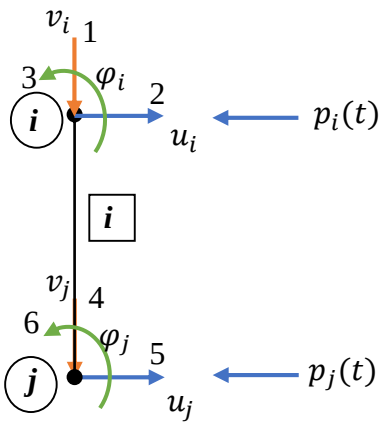

Figure 2.5 Degrees of freedom in a beam element

Other beam formulae that are needed in analyzing piles under lateral loads are:

$$V = EI\frac{d^3y_{rp}}{dx^3}$$

$$M = EI\frac{d^2y_{rp}}{dx^2}$$

$$S = \frac{dy_{rp}}{dx}$$

where

V = shear force perpendicular to the neutral axis [Note: $V_v = V - P_x\frac{dy_{rp}}{dx}$, if axial load is negligible then $V_v = V$],

M = bending moment in the pile, and

S = slope of the pile.

2.3 Numerical Modeling

In non-linear dynamics problems, a robust time stepping scheme is required that can damp the spurious effects of high frequency modes and converge quickly in order to improve the computational efficiency. The Hilber-Hughes-Taylor (HHT)-α method (Hilber et al., 1977), also called as the α-method (Hilber et al., 1977), is a widely used numerical integration scheme in structural dynamics. A precursor of the HHT-α method is the Newmark time integration method (Newmark et al., 1959). The HHT-α method has better accuracy and desirable numerical damping characteristics than the Newmark method. Muraleetharan et al. (1994) implemented HHT-α method-based time integration scheme to solve the governing non-linear equations of dynamic behavior of saturated soils.

In the following proposed numerical solution scheme, HHT-α method is combined with the Newton-Raphson method to solve the non-linear equations. The following algorithm is similar to the one developed and implemented in Muraleetharan et al. (1994), but here it is modified to solve the non-linear dynamic equations for soil structure interaction problem. Equation 2.12 can be modified as follows using the HHT-α method:

$$\mathbf{M}a_{n+1} + (1+\alpha)\mathbf{C}v_{n+1} - \alpha\mathbf{C}v_n + (1+\alpha)\mathbf{K_P}d_{n+1} - \alpha\mathbf{K_P}d_n + (1+\alpha)\mathbf{P}_{n+1} - \alpha\mathbf{P}_n$$

$$= (1+\alpha)(-\mathbf{M}\ddot{u}_{g_{n+1}}) - \alpha(-\mathbf{M}\ddot{u}_{g_n}) \qquad (2.14)$$

Here the subscript n denotes the n^{th} discrete time t_n and $\Delta t = t_{n+1} - t_n$ is the length of the representative time step. The 'n' ranges from zero to the total number of steps to be considered. In this case, $d_0, v_0, a_0, P_0, K_{T_0}$ and u_n are known.

The following Newmark's equations are retained in the HHT-α method:

$$v_{n+1} = v_n + [(1-\gamma)\Delta t]a_n + (\gamma \Delta t)a_{n+1} \tag{2.15}$$

$$d_{n+1} = d_n + (\Delta t)v_n + [(0.5-\beta)(\Delta t)^2]a_n + [\beta(\Delta t)^2]a_{n+1} \tag{2.16}$$

where α, β and γ are parameters that determine the stability and accuracy characteristics of the method. If α = 0, the HHT-α method reduces to the Newmark's method. Equations 2.14 to 2.16 are combined with the Newton-Raphson method and the following time stepping algorithm is developed, in which the iteration counter is denoted by a superscript in parenthesis that is $^{(i)}$.

If the relative pile deflection and relative soil displacement are known at any given time, the soil resistance and the tangent stiffness can be determined using dynamic *p-y* curves. As noted before, the relative soil displacement-time histories will be known prior to the analysis at all locations along the pile.

Step 1: Initialize the iteration counter *i* to zero

Step 2: Predictor

$$a_{n+1}{}^{(i)} = 0 \tag{2.17}$$

$$v_{n+1}{}^{(i)} = \overline{v_{n+1}} = v_n + [(1-\gamma)\Delta t]a_n \tag{2.18}$$

$$d_{n+1}{}^{(i)} = \overline{d_{n+1}} = d_n + (\Delta t)v_n + [(0.5-\beta)(\Delta t)^2]a_n \tag{2.19}$$

$$\mathbb{P}_{n+1}{}^{(i)} = \overline{\mathbb{P}_{n+1}} = b\mathbb{K}_T{}^{(i)}\left(d_{n+1}{}^{(i)} - u_{n+1}\right) \tag{2.20}$$

Step 3:

$$\Psi^{(i)} = f\left(a_{n+1}{}^{(i)}\right) = (1+\alpha)(-\mathbf{M}\ddot{u}_{g_{n+1}}) - \alpha(-\mathbf{M}\ddot{u}_{g_n}) - (1+\alpha)\mathbf{P}_{n+1}^{(i)} + \alpha\mathbf{P}_n - \mathbf{M}a_{n+1}^{(i)} -$$

$$(1+\alpha)\mathbf{C}v_{n+1}^{(i)} + \alpha\mathbf{C}v_n - (1+\alpha)\mathbf{K_P}d_{n+1}^{(i)} + \alpha\mathbf{K_P}d_n \qquad (2.21)$$

Step 4:

$$M_{eff}{}^{(i)} = \frac{-d\,f\left(a_{n+1}{}^{(i)}\right)}{d\left(a_{n+1}{}^{(i)}\right)} = \mathbf{M} + (1+\alpha)(\gamma\Delta t)\mathbf{C} + (1+\alpha)(\beta(\Delta t)^2)\mathbf{K_P} + (1+\alpha)(\beta(\Delta t)^2)b\mathbf{K_T}{}^{(i)}$$

(2.22a)

where $\mathbf{K_T}{}^{(i)} = \frac{\partial \mathbf{P}_{n+1}^{(i)}}{\partial(d_{n+1}{}^{(i)} - u_{n+1})}$ = global tangent stiffness matrix (2.22b)

Step 5:

Solve $\delta^{(i)} = -f\left(\mathrm{a}_{n+1}{}^{(i)}\right) / \left\{\frac{d\,f\left(a_{n+1}{}^{(i)}\right)}{d\left(a_{n+1}{}^{(i)}\right)}\right\} = \frac{\Psi^{(i)}}{M_{eff}{}^{(i)}} = \Delta a_{n+1}{}^{(i)}$ (2.23)

Step 6: Corrector

$$a_{n+1}{}^{(i+1)} = a_{n+1}{}^{(i)} + \delta^{(i)} \qquad (2.24)$$

$$v_{n+1}{}^{(i+1)} = \overline{v_{n+1}} + (\gamma\Delta t)a_{n+1}{}^{(i)} \qquad (2.25)$$

$$d_{n+1}{}^{(i+1)} = \overline{d_{n+1}} + (\beta(\Delta t)^2)a_{n+1}{}^{(i)} \qquad (2.26)$$

$$\mathbf{P}_{n+1}{}^{(i+1)} = b\mathbf{K_T}{}^{(i+1)}\left(d_{n+1}{}^{(i+1)} - u_{n+1}\right) \qquad (2.27)$$

Step 7:

$$\Psi^{(i+1)} = f\left(a_{n+1}{}^{(i+1)}\right) = (1+\alpha)(-\mathbf{M}\ddot{u}_{g_{n+1}}) - \alpha(-\mathbf{M}\ddot{u}_{g_n}) + (1+\alpha)\mathbf{P}_{n+1}^{(i+1)} - \alpha\mathbf{P}_n -$$

$$\mathbf{M}a_{n+1}^{(i+1)} - (1+\alpha)\mathbf{C}v_{n+1}^{(i+1)} + \alpha\mathbf{C}v_n - (1+\alpha)\mathbf{K_P}d_{n+1}^{(i+1)} + \alpha\mathbf{K_P}d_n \quad (2.28)$$

Step 8:

Convergence check: if $\frac{\|\Psi^{(i+1)}\|}{\|\Psi^0\|} < \varepsilon_1$ and $\frac{\|\Delta a_{n+1}{}^{(i)}\|}{\|a_{n+1}{}^{(i+1)}\|} < \varepsilon_2$ then go to next step else set $i = i+1$ and go to step 4.

This procedure will be used going forward.

Appendix. Matrix Terms

The element matrices for a prismatic 1D-beam element with the properties, element length (L), cross section area (A), mass density (ρ), Young's modulus (E), moment of inertia (I), and degrees of freedom shown in Figure 2.5 are given as following.

The pile stiffness matrix $[k_e]$ is given by,

$$[k_e] = \begin{bmatrix} \frac{EA}{L} & 0 & 0 & -\frac{EA}{L} & 0 & 0 \\ 0 & 12\frac{EI}{L^3} & 6\frac{EI}{L^2} & 0 & -12\frac{EI}{L^3} & 6\frac{EI}{L^2} \\ 0 & 6\frac{EI}{L^2} & 4\frac{EI}{L} & 0 & -6\frac{EI}{L^2} & 2\frac{EI}{L} \\ -\frac{EA}{L} & 0 & 0 & \frac{EA}{L} & 0 & 0 \\ 0 & -12\frac{EI}{L^3} & -6\frac{EI}{L^2} & 0 & 12\frac{EI}{L^3} & -6\frac{EI}{L^2} \\ 0 & 6\frac{EI}{L^2} & 2\frac{EI}{L} & 0 & -6\frac{EI}{L^2} & 4\frac{EI}{L} \end{bmatrix}$$

The mass matrix $[m_e]$ can be either lumped or consistent. The lumped mass matrix is given by,

$$[m_e] = \frac{\rho AL}{2}\begin{bmatrix} 1 & 0 & 0 & 0 & 0 & 0 \\ 0 & 1 & 0 & 0 & 0 & 0 \\ 0 & 0 & 1 & 0 & 0 & 0 \\ 0 & 0 & 0 & 1 & 0 & 0 \\ 0 & 0 & 0 & 0 & 1 & 0 \\ 0 & 0 & 0 & 0 & 0 & 1 \end{bmatrix}$$

The consistent mass matrix is given by,

$$[m_e] = \frac{\rho AL}{420}\begin{bmatrix} 140 & 0 & 0 & 70 & 0 & 0 \\ 0 & 156 & 22L & 0 & 54 & -13L \\ 0 & 22L & 4L^2 & 0 & 13L & -3L^2 \\ 70 & 0 & 0 & 140 & 0 & 0 \\ 0 & 54 & 13L & 0 & 156 & -22L \\ 0 & -13L & -3L^2 & 0 & -22L & 4L^2 \end{bmatrix}$$

The consistent mass matrix is used in the analysis.

The tangent stiffness matrix $[K_T]$ can be obtained from *p-y* curves, given by,

$$[K_T] = K_T \begin{bmatrix} 0 & 0 & 0 & 0 & 0 & 0 \\ 0 & 1 & 0 & 0 & 0 & 0 \\ 0 & 0 & 0 & 0 & 0 & 0 \\ 0 & 0 & 0 & 0 & 0 & 0 \\ 0 & 0 & 0 & 0 & 1 & 0 \\ 0 & 0 & 0 & 0 & 0 & 0 \end{bmatrix}$$

The analysis provides an option to include a seismic mass on top of the pile. This mass is assigned to node 1 (pile top node) as follows,

$$seismic\ mass * \begin{bmatrix} 1 & 0 & 0 \\ 0 & 1 & 0 \\ 0 & 0 & 1 \end{bmatrix}$$

The damping matrix can be expressed as a function of mass and stiffness of the pile. However, the significant damping comes from soil radiation damping and therefore no additional pile damping is considered in the analysis.

The relative pile acceleration, velocity and displacement vectors, a, v and d , respectively are given by,

$$d = \begin{pmatrix} u_1 \\ v_1 \\ \varphi_1 \\ \vdots \\ \vdots \\ u_i \\ v_i \\ \varphi_i \\ \vdots \\ \vdots \\ u_n \\ v_n \\ \varphi_n \end{pmatrix}_{dof\ x\ 1} \qquad v = \begin{pmatrix} \dot{u}_1 \\ \dot{v}_1 \\ \dot{\varphi}_1 \\ \vdots \\ \vdots \\ \dot{u}_i \\ \dot{v}_i \\ \dot{\varphi}_i \\ \vdots \\ \vdots \\ \dot{u}_n \\ \dot{v}_n \\ \dot{\varphi}_n \end{pmatrix}_{dof\ x\ 1} \qquad a = \begin{pmatrix} \ddot{u}_1 \\ \ddot{v}_1 \\ \ddot{\varphi}_1 \\ \vdots \\ \vdots \\ \ddot{u}_i \\ \ddot{v}_i \\ \ddot{\varphi}_i \\ \vdots \\ \vdots \\ \ddot{u}_n \\ \ddot{v}_n \\ \ddot{\varphi}_n \end{pmatrix}_{dof\ x\ 1}$$

CHAPTER 3: A METHOD TO CHARACTERIZE THE CDSM IMPROVED SOIL AROUND A PILE

3.1 Recent Lateral Load Testing of Piles in Improved Soils

Earthquakes have caused significant damage to civil engineering structures all over the world due to inadequate lateral load capacity and performance of pile foundations constructed in weak soils. The lateral load behavior of piles can be controlled by deploying a number of soil improvement techniques around piles such as surface compaction, chemical stabilization [e.g., Cement Deep Soil Mixing (CDSM) and grouting], vibroflotation, drainage methods, and precompression and consolidation. These soil improvement techniques enhance the strength and stiffness of soils and limits the lateral movement and distresses in piles during lateral loading.

The soil improvement techniques around piles have been proven to be effective and economical in practice to enhance the lateral strength and stiffness of weak soils in seismic regions compared to the traditional approach that increases the diameter and number of piles; however, literature on modeling of these soil improvement techniques are limited. CDSM is one such soil improvement technique that has been extensively used for seismic strengthening of many pile foundations, but has limited literature available related to modeling.

Recently the CDSM was proven to be an effective solution for improving the lateral loading behavior of piles in soft clays through centrifuge (Liu et al., 2016) and full-scale field tests (Fleming et al., 2016). Further, Ohtsuka et al. (2004) proved analytically that the CDSM improvement around a pile is an economical design in weak soils. A study conducted as a part of the NEES-pilEs (Network for Earthquake Engineering Simulation-piles in low E soils) project

attempted to model the seismic soil-pile interaction responses in CDSM improved soils using the LPILE computer program and a fully-coupled finite element computer code, TeraDysac (Muraleetharan et al., 2003; Kirupakaran et al., 2010; Sritharan and Huang, 2010; Taghavi and Muraleetharan, 2012; Quiroga et al., 2017).

As a part of the NEES-pilEs project, Fleming et al. (2016) tested identical full-scale single piles in CDSM improved and unimproved soft clays under pseudo-static and cyclic loading conditions. The results revealed that the CDSM improved ground showed a 42% increase in the lateral resistance, and a 600% increase in the effective lateral stiffness over the unimproved soft clay.

Liu et al. (2016) conducted pseudo-static and seismic tests on single piles in CDSM improved and unimproved soft clays for the NEES-pilEs project. The results showed that a ground improvement of 13D x 13D x 9D (length x width x depth) around a pile, where D is the outer diameter of the pile, is effective in limiting the lateral displacements and accelerations. Taghavi et al. (2017) performed seismic tests on group piles using seven different earthquake events with peak accelerations ranging from 0.03 to 0.66g. The observations showed that the pile cap displacements or accelerations depend on the frequency content of the input base motion. Moreover, small improvement dimensions resulted in higher pile top accelerations compared to both the large and no soil improvement dimensions. This showed that the improvement dimensions are critical for the lateral loading behavior of piles (Taghavi et al., 2017).

3.2 Previous Work on CDSM Modeling

Sritharan and Huang (2010) assumed that the CDSM improved soft clay and the unimproved soft clay under static loading behave as two non-linear spring elements connected in series (Figure 3.1) and then modeled this as a single homogenized non-linear spring using their compounded properties of the springs to represent the combined behavior. The *p-y* curve for the compounded homogenized spring was developed by modifying the *p-y* curve of the unimproved soil by a G-multiplier (G_m). G_m is given by the ratio between effective stiffness of the homogenized equivalent spring and the initial stiffness of soft clay. The modified *p-y* curve was used as an input in the LPILE computer program to represent the combined non-linear behavior of CDSM and the surrounding unimproved soft clay and the pile responses were predicted. However, the method proposed by Sritharan and Huang (2010) was based on the initial stiffness of the CDSM improved and unimproved soft clay. Note that the initial stiffness cannot fully represent the non-linear soil behavior when subjected to a lateral dynamic loading.

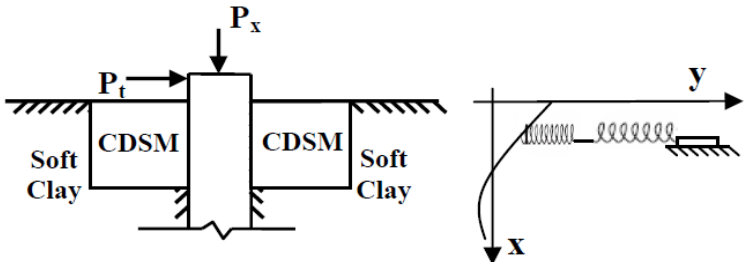

Figure 3.1 Springs in series to account for soil improvement around a pile (from Sritharan and Huang, 2010)

Fleming et al. (2012) further improved the method proposed by Sritharan and Huang (2010) by incorporating the idea recommended by Guo and Lee (2001). This method employs radial attenuation factors on the pile displacement and soil resistance of the improved soil to account for the decrease of pile displacement and soil resistance in the direction of loading. The

attenuation factors were input as a function of depth in the LPILE program and the effects of soil improvement dimensions were investigated. It was found that the increasing soil improvement depth up to the point where zero bending moment occurs in the pile will decrease the lateral displacements of the pile. Furthermore they found that the CDSM improvement beyond the zero moment point becomes ineffective, but increasing the soil improvement width is an efficient way to decrease the lateral displacements of the pile (Fleming et al., 2012).

A fully-coupled finite element computer code, TeraDysac (Muraleetharan et al., 2003), with a bounding surface constitutive model was used to predict the seismic soil-pile interaction in CDSM improved soils (Kirupakaran et al., 2010; Taghavi and Muraleetharan, 2012). In this study, an artificial Over Consolidation Ratio (OCR) (Thompson, 2011) was used to simulate the over-consolidation effects of cementitious CDSM block around piles.

Simple computer programs are available to analyze the pile foundation under static and cyclic loading, but not under dynamic loading. Moreover, these computer programs do not account for lateral extent of the improved soil. Finite element computer codes based on fully coupled continuum models, on the other hand can make reasonable predictions, but are complicated and time consuming and are therefore not convenient for day-to-day designs.

3.3 Proposed Method to Characterize CDSM around Piles

The Winkler analysis is a popular concept and a simplified approach used by practicing engineers to analyze soil-structure interaction problems, however, the original method is incapable of modeling two types of soils in a layer due to its one-dimensional assumptions. The LPILE program which is a non-linear extension of the original Winkler model is also not capable

of modeling the improved and unimproved soil in a single layer. The objective is to develop a method to characterize the lateral load behavior of the combined layer using the Winkler approach. A method is proposed in this section to modify the parameters used to model the *p-y* curves in the LPILE program.

The following *p-y* formulations are listed in the LPILE to model the stiff clay behavior

(1) stiff clay with free water,

(2) stiff clay with no free water, and

(3) modified *p-y* formulation for stiff clay with no free water.

Although in centrifuge tests of Liu et al. (2016), the CDSM improved layer was under water, stiff clay with free water model is not used here because it considers scour formation around the pile, but under limited pseudo-static loading, scour formation in CDSM is very unlikely. Stiff clay without free water has been used successfully for many years to model the stiff clay behavior, however, there have been incidents reported from the Southeastern United States where full-scale load tests on piles have identified that the initial stiffness of the load-deflection response modeled using this formulation is too steep. Therefore, the latest modified *p-y* formulation for stiff clay with no free water model is used to characterize the CDSM improved soft clay. The modified *p-y* curve overcame the steep initial stiffness issue by requiring this stiffness value as an input.

In the modified *p-y* formulation for stiff clay, the following additional modifications are proposed for the initial soil stiffness (k) and undrained shear strength (S_u):

Modified soil stiffness $(k_{mod}) = \frac{L.k}{30D}$ (4.1)

Modified undrained shear strength $(S_{u,mod}) = \frac{L.S_u}{30D}$ (4.2)

where L and D are lateral dimension of the improved zone and the pile diameter, respectively. In a CDSM improved soil layer, the effect of unimproved soft clay on stiffness and ultimate strength of the layer is negligible when compared to the CDSM improved clay section for typical improvement dimensions. Therefore, the above given factors consider modifications only for k and S_u of CDSM improved clay.

Using the centrifuge test data that will be discussed later, a parametric study varying the lateral extent from 15D to 35D was performed to find the length of a semi-infinite (one-dimensional) layer. The pile responses for a selected lateral load of 27.7 kN and for an actual improvement dimension of 9D x 9D x 6D (measured) and various scaling lengths are shown in Figure 3.2. For example, F20 denotes a lateral dimension of the improved zone of 20D is used in Equations 4.1 and 4.2 instead of 30D. The changes in pile responses were negligible for a length greater than 28D and overall the LPILE-predicted responses were in good agreement with the measured values. These types of comparisons were also done for other measured pile responses with 13D x 13D x 9D and 17D x 17D x 12D improvements. Based on all of these comparisons a scaling length of 30D was chosen. Essentially this imply when the lateral dimensions of the improvement is beyond 30D, the improved layer behaves as a semi-infinite layer.

According to the LPILE Technical Manual, stiff to hard clays are characterized as those clays with undrained shear strength between 200 to 400 kPa. The recommended k and strain factor (ε_{50}) values for these clays are 540,000 kN/m^3 and 0.004, respectively. These values were used to model the *p-y* curves of the CDSM layer with the above proposed modifications.

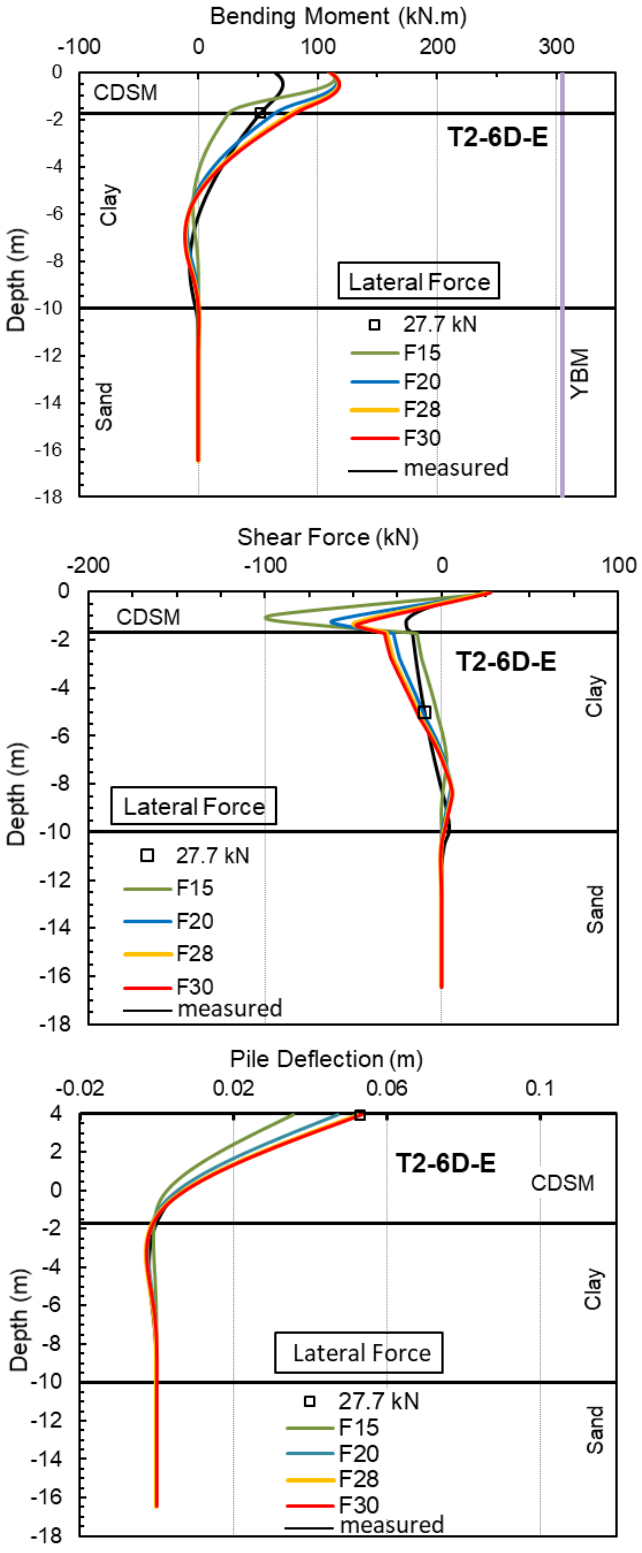

Figure 3.2 Measured and LPILE-predicted pile responses for an actual improvement depth of 6D and for a selected lateral load of 27.7 kN

3.4 Validation of the Proposed Method using Centrifuge Test Results

3.4.1 *Overview of Pseudo-static Tests*

As a part of NEES-pilEs centrifuge tests, a series of pseudo-static loading tests were conducted on the improved and unimproved piles (Liu et al., 2016). The pile heads were laterally loaded in a displacement controlled manner to a target displacement. Two piles from Test #1 and four piles from Test #2 were tested for pseudo-static loads. The pile properties are listed in Table 3-1. The piles were labeled as shown in Figures 3.4 through 3.7. The first two characters in the label refer to the test number (Test #1 or Test #2), the second two characters refer to the depth of CDSM improvement (UI refers to unimproved case), and the last letter refers to the east or west side of the centrifuge box. For example, T1-9D-W denotes the Test #1 pile on the west side with soil improvement dimensions of 13D x 13D x 9D where D is the outside diameter of the pile.

Table 3-1 Properties of test piles (from Liu et al., 2016)

Centrifuge test no.	Material	Outside diameter, D, (mm)	Wall thickness, t, (mm)	Length (mm)	Young's modulus, E, (GPa)	Yield strength (MPa)	Yield bending moment (kN.m)
1	Aluminum	476	27	18,288	66.1	167.5	763
2	Steel	286	27	20,388	192.5	260.0	305

A cubic spline curve fitting procedure was used to interpolate the bending moments between the discrete values of bending moments obtained from the strain gauge data. The details are explained in Soltani (2016). Shear forces were then determined by differentiating the bending moments with respect to depth and pile deflections were obtained by integrating the bending moment curves along the piles (assuming a constant EI for the pile).

3.4.2 LPILE Modeling

The LPILE simulations require input information on the soil properties and stratigraphy, pile properties, and boundary conditions. A combination of centrifuge test data and *p-y* parameters using the proposed method were used to create the LPILE model. The *p-y* curves for soft clay and dense sand were generated using Matlock (1970) and Reese, et al. (1974), respectively, with the parameters listed in Table 3-2. The CDSM improved soft clay was modeled in LPILE using the modified *p-y* formulation for stiff clay with no free water by Welch and Reese (1975) with the model parameters listed in Table 3-3 obtained using Equations 4.1 and 4.2.

Table 3-2 Soil properties used in LPLIE analyses

Soil type	***p-y* curve in LPILE**	**ɣ′ (kN/m^3)**	**S_u (kPa)**	**ε_{50}**	**ϕ (^{0})**	***k* (kN/m^3)**
CDSM	Modified stiff clay without free water	8.69	330	0.004	-	540,000
Soft clay	Matlock (1970)	8.18	2.71-24.1	0.02	-	-
Dense Sand	Reese, et al. (1974)	10.44	-	-	38	33,900

Table 3-3 Modified parameters used in stiff clay model in LPILE

Improvement case	***L***	**k_{mod} (kN/m^3)**	**$S_{u,mod}$ (kPa)**	**ε_{50}**
6D	9D	162,000	99	0.004
9D	13D	234,000	143	0.004
12D	17D	306,000	187	0.004

The pile behavior was modeled using the elastic properties listed in Table 3-1. Limited number of analyses were also carried out using non-linear moment-curvature curves obtained by coupon tests and fiber pile analyses (personal communication with Sri Sritharan, Iowa State University, 2013). The moment-curvature curves are shown in Figure 3.3.

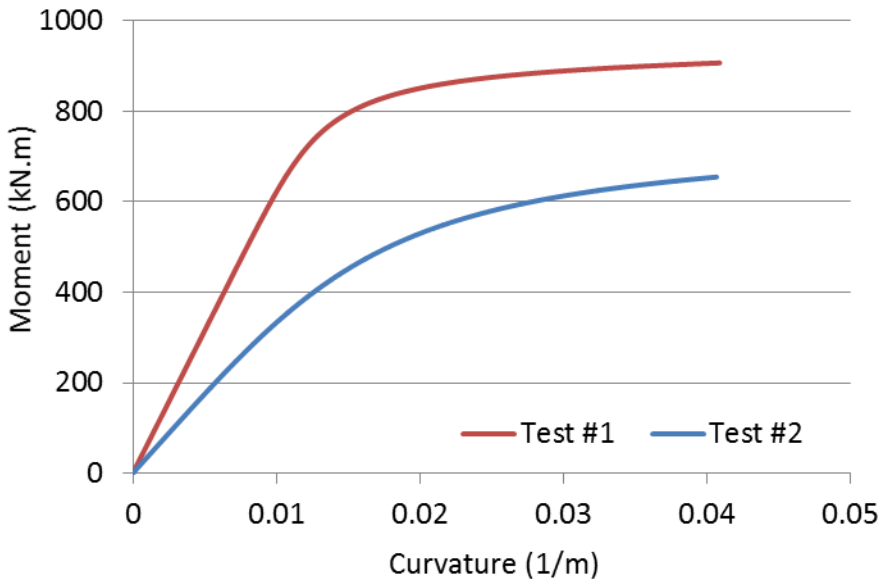

Figure 3.3 Moment-curvature curves used in LPILE analyses

The measured lateral loads in the centrifuge tests were applied at the pile heads in LPILE model and the resulting bending moments, shear forces and pile deflections were predicted. The comparisons from linear analyses are shown in the Figures 3.4, 3.5, and 3.6. Note that, as mentioned previously, the measured curves were obtained through a cubic spline curve fitting method. The comparisons from non-linear analyses are shown in the Figure 3.7 for Test #2, 9D improved case and for loadings 90.5 kN and 137.9 kN.

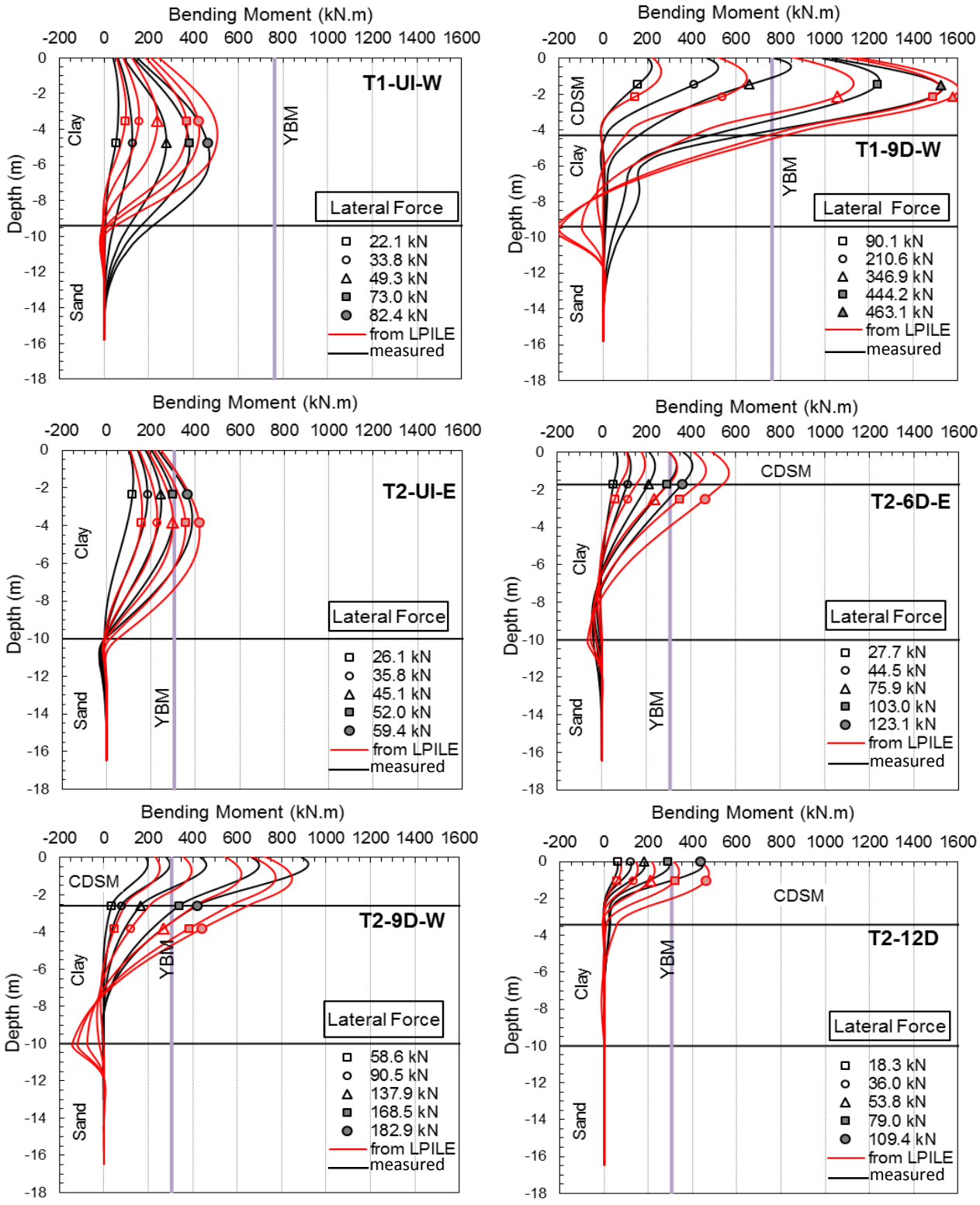

Figure 3.4 Measured and LPILE-predicted bending moment distributions for piles in Test #1 and Test #2

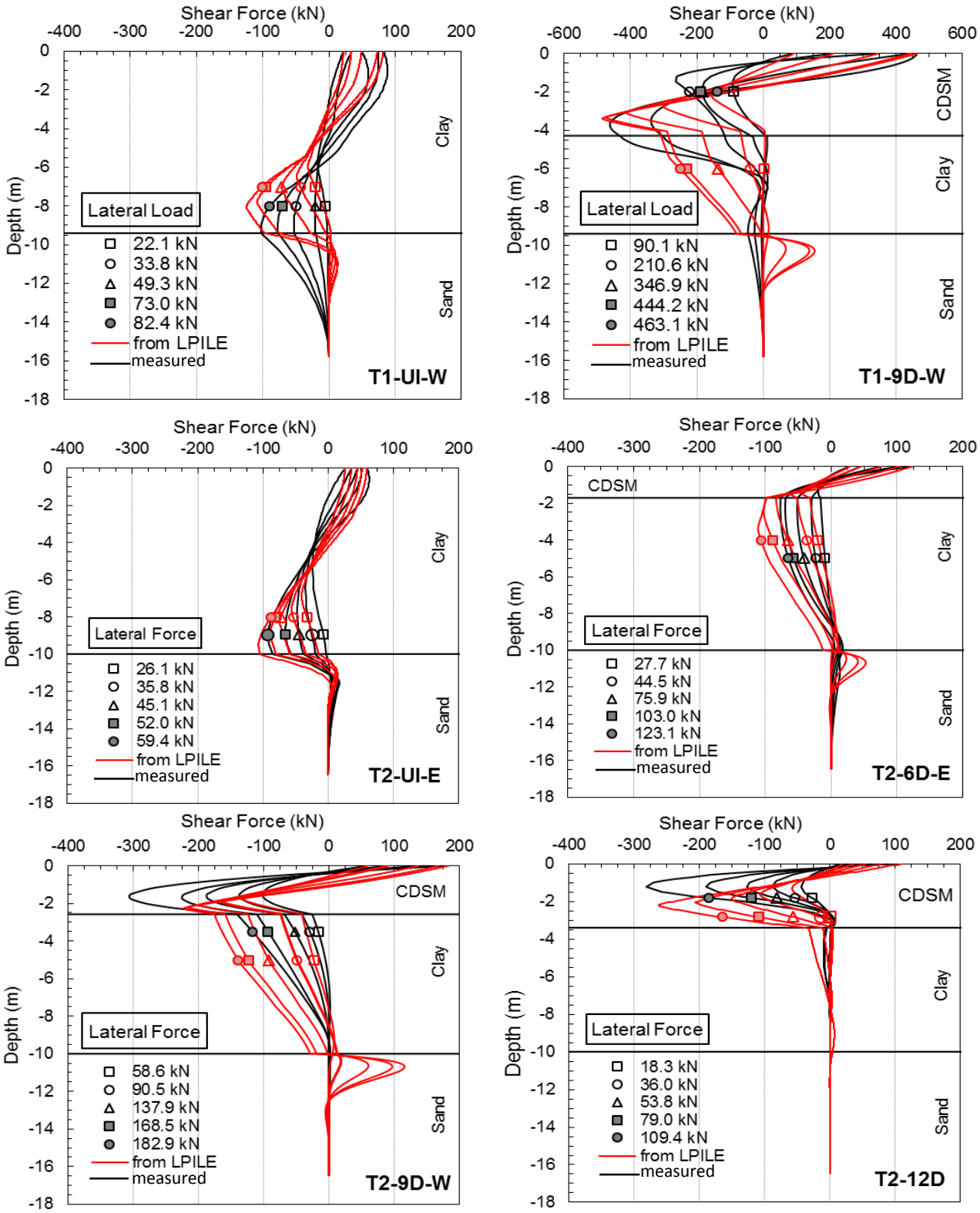

Figure 3.5 Measured and LPILE-predicted shear force distributions for piles in Test #1 and Test #2

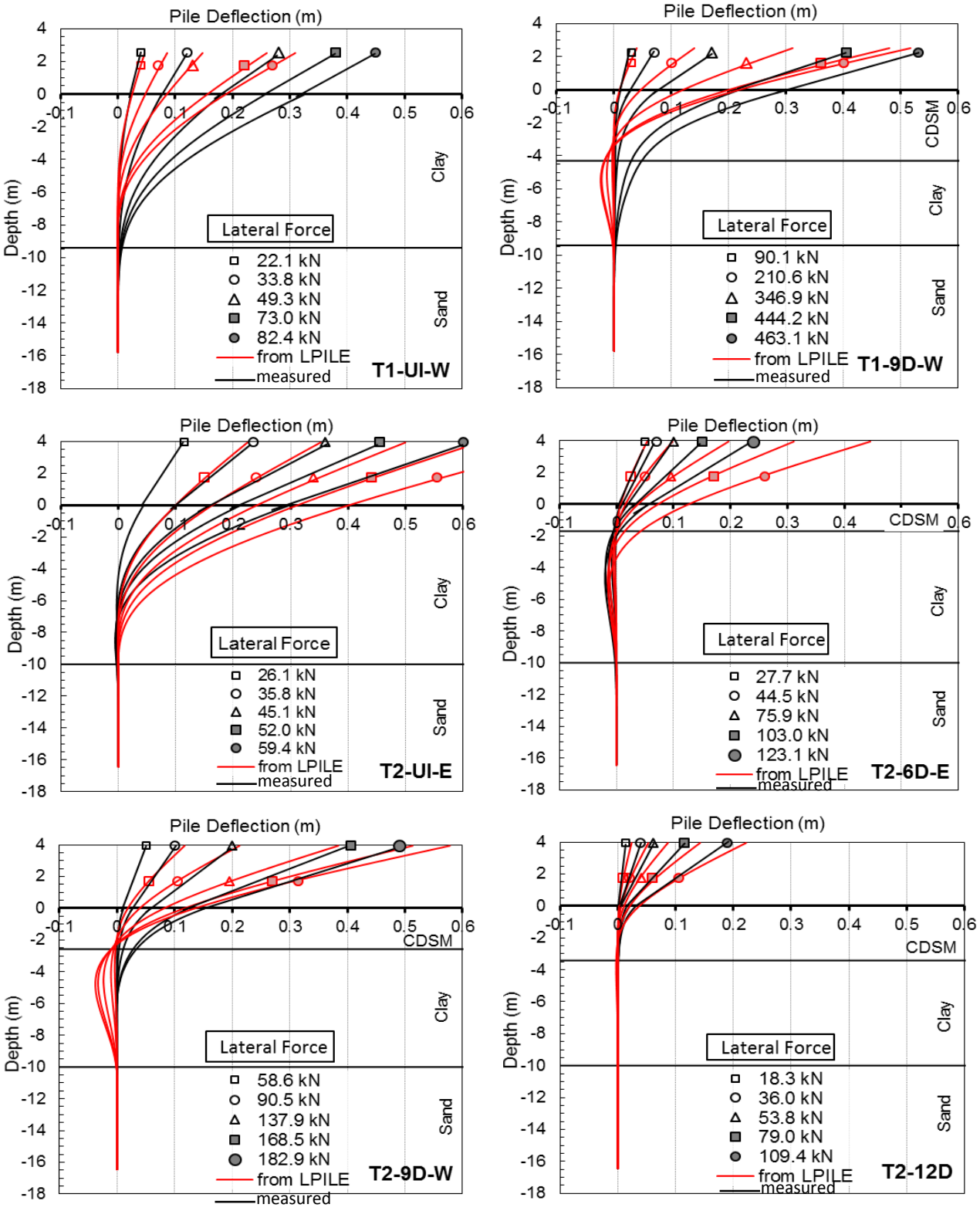

Figure 3.6 Measured and LPILE-predicted pile deflections for piles in Test #1 and Test #2

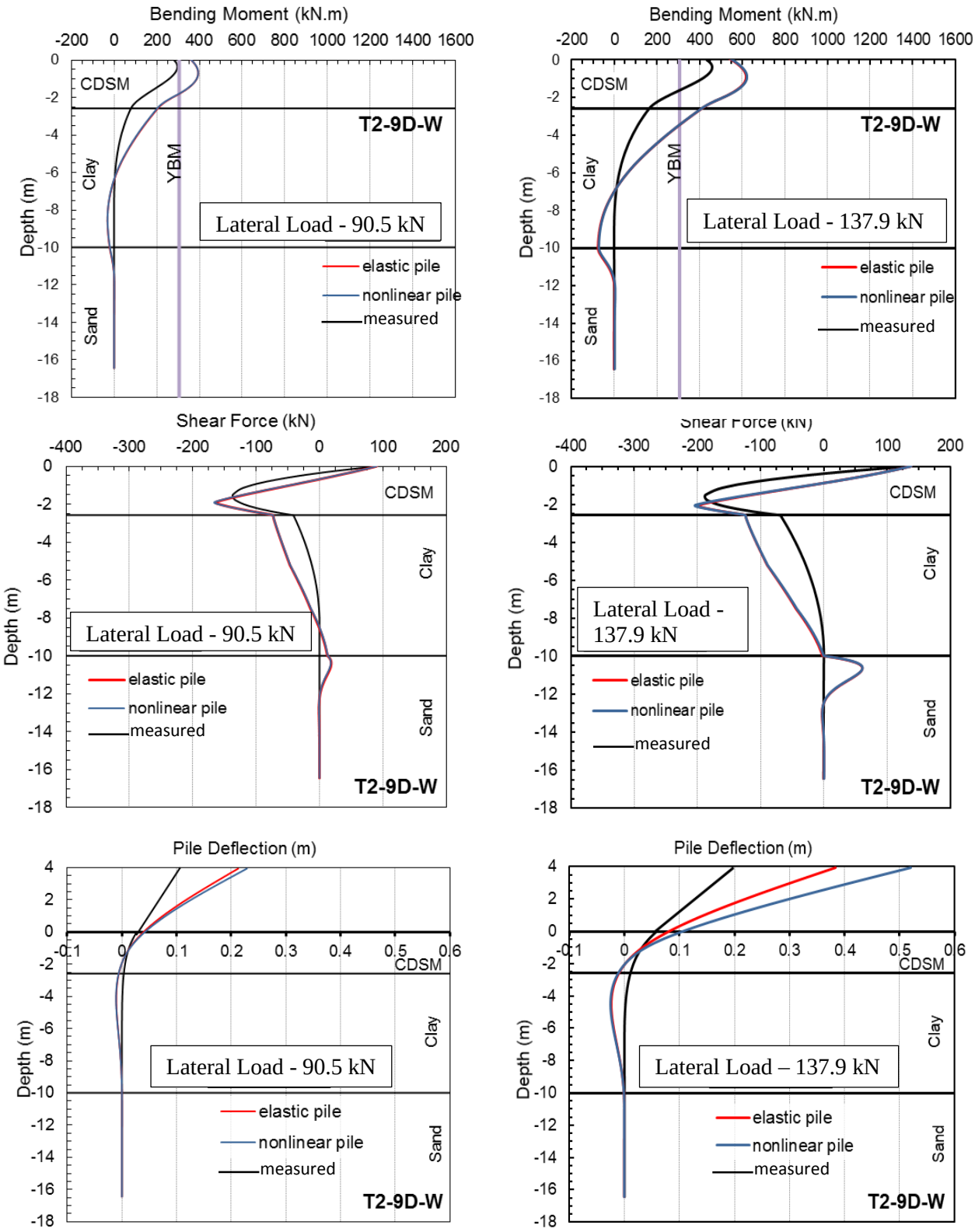

Figure 3.7 Measured and LPILE-predicted pile responses using non-linear pile sections

3.4.3 Comparisons between Measured and LPILE-predicted Values

Linear and non-linear pile sections were modeled in the LPILE program and were subjected to the lateral loads of 90.5 kN and 137.9 kN. The non-linear analyses did not converge for loads larger than 137.9 kN and therefore are not reported here. The resulting pile responses are plotted in Figure 3.7. The bending moments and shear forces look the same. This is because, for lower loads, the pile bending stiffness used in non-linear model is similar to the one in the linear model. The differences in pile deflections for linear and non-linear analyses are larger for the lateral load of 137.9 kN than 90.5 kN. This is likely because plastic deformation increases as the lateral load increases.

The LPILE-predicted results are compared with the measured values that are plotted in Figures 3.4, 3.5, and 3.6 (i.e., linear pile sections), using a quantitative measure called root-mean-square error (RMSE) that is calculated using the following equation:

$$RMSE = \sqrt{\frac{\sum_{i=1}^{n}(\hat{y}_i - y_i)^2}{n}} \tag{3.3}$$

where y_i is the measured value for the i^{th} depth, $\hat{y}_i$ is the LPILE-predicted value, and n is the total number of points considered along the pile. The RMSE values are computed for each improvement case and for each lateral load separately and listed in Tables 3-4 through 3-6. These values are categorized as within the elastic region and when yielding that is based on the yield bending moments (YBM) listed in Table 3-1 and shown in Figure 3.4, which are 763 kN.m and 305 kN.m for Test #1 and Test #2, respectively. Table 3-7 shows the average RMSE values of pile bending moments, shear forces, and deflections. Finally, the computed RMSE values are listed as a percentage of maximum value of respective measured response quantity in Table 3-8.

Table 3-4 RMSE values between measured and predicted bending moments

		within elastic region					
T1-UI-W	Lateral Force (kN)	22.1	33.8	49.3	73	82.4	95.9
	RMSE (kN.m)	21.5	33.9	63.3	70.8	90.5	110.8
T1-9D-W	Lateral Force (kN)	90.1	210.6	-	-	-	-
	RMSE (kN.m)	32.1	132.9	-	-	-	-
T2-UI-E	Lateral Force (kN)	26.1	35.8	45.1	-	-	-
	RMSE (kN.m)	36.5	35.6	41.5	-	-	-
T2-6D-E	Lateral Force (kN)	27.7	44.5	75.9	-	-	-
	RMSE (kN.m)	25.3	34.3	61.5	-	-	-
T2-9D-W	Lateral Force (kN)	58.6	90.5	-	-	-	-
	RMSE (kN.m)	46.9	92.2	-	-	-	-
T2-12D	Lateral Force (kN)	18.3	36	53.8	-	-	-
	RMSE (kN.m)	8.4	24.4	44.7	-	-	-

		when yielding			
T1-UI-W	Lateral Force (kN)	-	-	-	-
	RMSE (kN.m)	-	-	-	-
T1-9D-W	Lateral Force (kN)	346.9	444.2	463.1	460.5
	RMSE (kN.m)	309.1	235.1	149.0	168.5
T2-UI-E	Lateral Force (kN)	52	59.4	63.2	-
	RMSE (kN.m)	42.0	37.1	33.7	-
T2-6D-E	Lateral Force (kN)	103	123.1	143.4	-
	RMSE (kN.m)	90.6	121.6	126.0	-
T2-9D-W	Lateral Force (kN)	137.9	168.5	182.9	188.6
	RMSE (kN.m)	166.7	141.3	140.9	170.1
T2-12D	Lateral Force (kN)	79	109.4	131.6	-
	RMSE (kN.m)	67.6	105.5	126.0	-

Table 3-5 RMSE values between measured and predicted shear forces

		within elastic region					
T1-UI-W	Lateral Force (kN)	22.1	33.8	49.3	73	82.4	95.9
	RMSE (kN)	6.6	12.9	22.7	25.3	31.3	37.2
T1-9D-W	Lateral Force (kN)	90.1	210.6	-	-	-	-
	RMSE (kN)	27.8	74.9	-	-	-	-
T2-UI-E	Lateral Force (kN)	26.1	35.8	45.1	-	-	-
	RMSE (kN)	13.8	13.1	13.9	-	-	-
T2-6D-E	Lateral Force (kN)	27.7	44.5	75.9	-	-	-
	RMSE (kN)	10.0	12.9	17.4	-	-	-
T2-9D-W	Lateral Force (kN)	58.6	90.5	-	-	-	-
	RMSE (kN)	19.4	32.5	-	-	-	-
T2-12D	Lateral Force (kN)	18.3	36	53.8	-	-	-
	RMSE (kN)	6.3	23.3	43.3	-	-	-

		when yielding			
T1-UI-W	**Lateral Force (kN)**	-	-	-	-
	RMSE (kN)	-	-	-	-
T1-9D-W	Lateral Force (kN)	346.9	444.2	463.1	460.5
	RMSE (kN)	159.4	97.0	92.1	127.8
T2-UI-E	Lateral Force (kN)	52	59.4	63.2	-
	RMSE (kN)	12.0	9.5	11.4	-
T2-6D-E	Lateral Force (kN)	103	123.1	143.4	-
	RMSE (kN)	22.4	27.8	27.4	-
T2-9D-W	Lateral Force (kN)	137.9	168.5	182.9	188.6
	RMSE (kN)	59.8	76.3	111.2	147.2
T2-12D	Lateral Force (kN)	79	109.4	131.6	-
	RMSE (kN)	72.5	106.9	144.6	-

Table 3-6 RMSE values between measured and predicted deflections

		within elastic region					
T1-UI-W	Lateral Force (kN)	22.1	33.8	49.3	73	82.4	95.9
	RMSE (m)	0.001	0.019	0.058	0.064	0.086	0.106
T1-9D-W	Lateral Force (kN)	90.1	210.6	-	-	-	-
	RMSE (m)	0.002	0.006	-	-	-	-
T2-UI-E	Lateral Force (kN)	26.1	35.8	45.1	-	-	-
	RMSE (m)	0.030	0.034	0.047	-	-	-
T2-6D-E	Lateral Force (kN)	27.7	44.5	75.9	-	-	-
	RMSE (m)	0.001	0.004	0.007	-	-	-
T2-9D-W	Lateral Force (kN)	58.6	90.5	-	-	-	-
	RMSE (m)	0.003	0.007	-	-	-	-
T2-12D	Lateral Force (kN)	18.3	36	53.8	-	-	-
	RMSE (m)	0.000	0.001	0.002	0.002	-	-

		when yielding			
T1-UI-W	Lateral Force (kN)	-	-	-	-
	RMSE (m)	-	-	-	-
T1-9D-W	Lateral Force (kN)	346.9	444.2	463.1	460.5
	RMSE (m)	0.016	0.033	0.062	0.085
T2-UI-E	Lateral Force (kN)	52	59.4	63.2	-
	RMSE (m)	0.058	0.063	0.063	-
T2-6D-E	Lateral Force (kN)	103	123.1	143.4	-
	RMSE (m)	0.018	0.033	0.068	-
T2-9D-W	Lateral Force (kN)	137.9	168.5	182.9	188.6
	RMSE (m)	0.015	0.026	0.031	0.033
T2-12D	Lateral Force (kN)	79	109.4	131.6	-
	RMSE (m)	0.0	0.006	0.008	-

Table 3-7 Average RMSEs between measured data and predictions

Pile response	RMSE within elastic region		RMSE when yielding	
	Test #1	Test #2	Test #1	Test #2
Bending moment (kN.m)	82	45	215	122
Shear force (kN)	51	21	119	58
Deflection (m)	0.004	0.003	0.049	0.024

Table 3-8 Percentage (%) between RMSE and maximum values

Pile response	% within elastic region		% when yielding	
	Test #1	Test #2	Test #1	Test #2
Bending moment	16.5	15.1	13.5	13.2
Shear force	19.0	15.4	23.8	19.4
Deflection	4.0	3.0	9.0	6.0

The relative pile-soil stiffness is a crucial factor in determining the lateral load performance of pile foundations. The LPILE-predicted values with modified *p-y* curves are directly relevant to systems with similar pile-soil relative stiffness values. A dimensionless-parameter, $(EI/At)/S_uD$, mentioned in the study by Taghavi et al. (2017) is used to capture the relative stiffness of the pile–soil system. The pile–soft clay and pile–CDSM relative stiffness values for both Tests #1 and #2 are listed in the Table 3-9. It can be seen that Test #2 has slightly stiffer pile-soil system than Test #1. The percentage deviation of RMSE are slightly smaller for Test #2 than Test #1.

Table 3-9 Relative stiffness of pile-soil system

Centrifuge Test no.	Cross-sectional area, A (mm^2)	Moment of inertia, I (mm^4)	Relative stiffness of pile-soil system, $(EI/At)/(S_uD)$	
			pile-soft clay	pile-CDSM
1	38,086	9.63E+08	1.76E+07	3.94E+05
2	21,969	1.86E+08	2.86E+07	6.40E+05

The LPILE-predicted values are in the range of ± 15 to 20 % from the peak values of the respective measured curves for both within the elastic region and when yielding. The predictions made by the elastic pile properties and the proposed *p-y* modification method are in closer agreement with the measured responses for lower load cases and within the elastic region. For higher load cases, when the pile likely begins to yield, the predictions have higher RMSE values but the % RMSEs remain lower. Therefore, it can be concluded that the proposed method reasonably accounts for CDSM improved soil around the pile and capable of predicting the pile responses better under lower pseudo-static loads, i.e., when the piles remain elastic.

3.5 Proposed Method for Cyclic and Dynamic Loading

The important factor to consider under cyclic and dynamic loading is the formation of gap (scour). If there is a potential for scouring of soil, either due to higher water table in a fissured soil or higher loading, the stiff clay with free water curve is recommended for modeling CDSM improved soft clay with proposed modifications in Section 3.3. Otherwise, modified stiff clay model without free water is recommended.

The seismic *p-y* curve for CDSM improved clay was developed by modifying the original model recommended by Boulanger et al. (1999). The Boulanger et al. (1999) model for

clay requires five inputs that are (1) ultimate soil resistance (p_{ult}), (2) relative pile displacement at 50% of ultimate soil resistance (y_{50}), (3) soil type (1 for clay or 2 for sand), (4) a drag coefficient, and (5) a dashpot coefficient. The p_{ult} and y_{50} are found from the backbone curves generated by the LPILE program for CDSM improved soft clay that is modeled using the proposed method in Section 3.3. The resulting seismic *p-y* curve parameters are input into DYPAC (Dynamic Piles Analysis Code program) that will be introduced and explained in Chapter 4. An example of input parameters at a selected depth is listed in Table 3-10.

Table 3-10 An example of input parameters for Boulanger et al. (1999) *p-y* curve at a depth of 1.16 m

Improvement case	p_{ult} (kN/m^2)	y_{50}	Soil type	Drag	Dashpot
6D	136.33	0.0038	1	0.1	0.5
9D	198.54	0.0040	1	0.1	0.5
12D	259.24	0.0045	1	0.1	0.5

3.6 Summary and Findings

A simple method is proposed and validated to assist the practicing engineers in modeling the pseudo-static lateral load behavior of a single pile in improved soils. The input parameters are directly obtained from in-situ or lab soil tests. The traditional and popular Winkler analysis approach is used to provide the simple solution. The CDSM improved soft clay is modeled using the modified formulation for stiff clay with additional modifications for initial soil stiffness (k) and undrained shear strength (S_u). A parametric study varying the lateral extent from 15D to 35D was performed and a length equal to or greater than 30D is found to adequately represent a semi-infinite layer. Using the proposed modifications, the pseudo-static pile responses in CDSM improved soft clay were predicted using the LPILE program. The LPILE-predicted values are

compared with the centrifuge test results of Liu et al. (2016) and the following conclusions are made:

- The proposed method reasonably accounts for CDSM improved soil around the pile and capable of predicting the pile responses under lower pseudo-static loads before yielding of piles. The root-mean-square errors as a percentage of the respective measured peak values are in the range of ± 15 to 20 % for linear analyses.

- The close agreement between the LPILE-predicted pile deflections (± 6%) with the measured values confirm that the proposed method for modifying the *p-y* curve is reasonable, at lower loads, especially when piles have not yielded.

CHAPTER 4: VALIDATION OF THE NON-LINEAR WINKLER MODEL

The numerical model developed in Chapter 2 is implemented into a finite element computer code called DYPAC (Dynamic Piles Analysis Code) using FORTRAN programming language. DYPAC can predict the soil-structure interaction responses in unimproved and improved soils under seismic loading. In this chapter, details of DYPAC program are provided and the predictions made by this computer code are validated using centrifuge test results.

4.1 Overview of Centrifuge Tests

The centrifuge tests that are used here were conducted at the NEES@UC Davis-Center for Geotechnical Modeling centrifuge facility as a part of the NEES-pilEs project (Liu et al., 2016). The centrifuge model consisted of a container made out of aluminum flexible shear beam rings, a base plate carrying the container, a shaking table, and a reaction mass. The soil-pile model was constructed inside the container. A total of 14 single piles were tested in two centrifuge tests subjected to pseudo-static and seismic loading. Two piles in each test were constructed in unimproved soft clay and the rest were constructed in CDSM improved ground with different soil improvement dimensions.

The properties of the piles used in Test #1 and Test #2 are shown in Table 3-1 in Section 3.4.1. In Test #1, the aluminum tubes used had 35% higher flexural strength than that of piles used by California Department of Transportation (Caltrans); therefore, in Test #2, less stiffer steel tubes were selected that had similar yielding behavior to steel pipe piles used in seismic zones by Caltrans. The soil properties used in Test #2 are listed in Table 4-1. The soil profile consisted of four layers of clay (total thickness 10 m) underlain by two layers of dense sand

(total thickness 8 m). These pile and soil properties are used as inputs in DYPAC analyses.

Table 4-1 Soil properties used in Centrifuge Test #2 (from Soltani, 2016)

Soil	Thickness (m)	Undrained shear strength (kPa)	Effective unit weight (kN/m^3)	Strain factor, ε_{50}	K (kN/m^3)
4th Clay layer	2.742	2.78-5.38	8.18	0.002	-
3rd Clay layer	2.490	8.61-9.86	8.68	0.002	-
2nd Clay layer	2.250	14.03-15.15	9.05	0.002	-
1st Clay layer	2.520	19.34-20.57	9.28	0.002	-
2nd Sand	3.810	-	10.88	-	33,900
1st Sand	4.230	-	10.44	-	33,900

The layout of Test #2 is shown in Figure 4.1. The ground improvement around the single piles consisted of one large (17D×17D×12D), two medium (13D×13D×9D), and two small (9D×9D×6D) zones, where D is the outer diameter of the pile. The dimensions of the improved zone are given as length×width×depth. One of the two identical models for the piles improved by the small and medium zones was tested under pseudo-static and the other was tested under seismic loading. Other important aspects and results of the centrifuge tests are explained in Liu et al. (2016) and Soltani (2016). Pseudo-static results have already been utilized and discussed in Chapter 3.

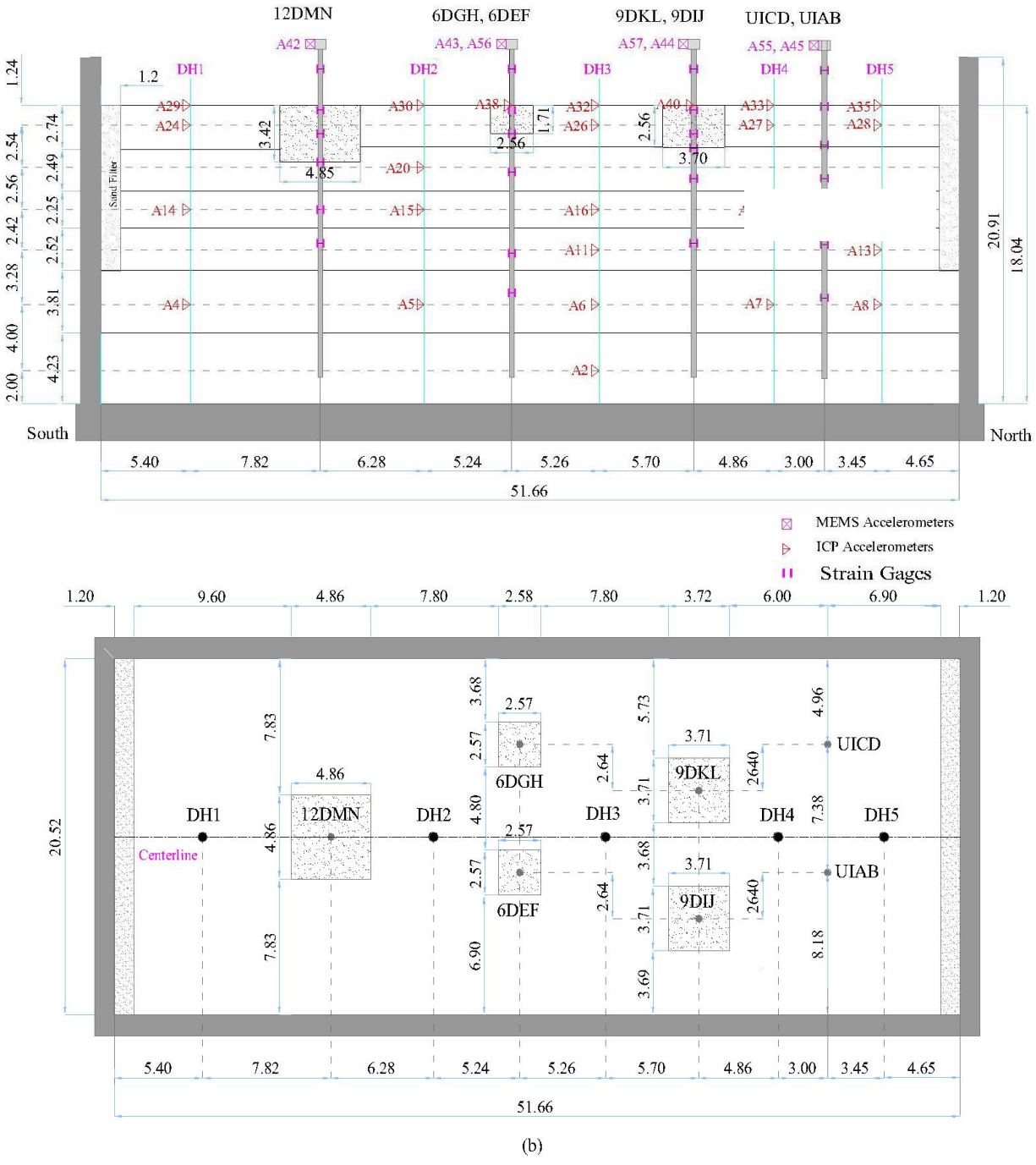

Figure 4.1 Centrifuge model layout (a) side view (b) plan view (prototype dimensions in meters, from Soltani, 2016)

4.2 DYPAC Modeling

DYPAC is a one-dimensional, finite element computer code that predicts the seismic responses of single piles in unimproved and CDSM improved soils. It solves the non-linear, dynamic governing equations presented in Chapter 2. In the validation analyses presented here, a single pile was modeled with 100 (user input) linear elastic beam elements (81 below ground and 19 above). Each of the 82 pile nodes below the ground surface was connected to one non-linear *p-y* element. The soil behavior was represented by non-linear *p-y* springs and viscous dashpots to simulate the soil-pile yielding, gapping, radiation damping, and soil cave-in and recompression as discussed in Section 4.3. As a first step, it was assumed that the damping was caused by soil only and the pile damping was neglected.

The displacement time histories from the free-field site response analyses were input to the free-field ends of the non-linear *p-y* elements as discussed in Section 4.5. The numerical integration consisted of Newton-Raphson iteration and the Hilber-Hughes-Taylor α-method (Hilber et al. 1977) with $\alpha = -0.3, \beta = 0.4225,$ and $, \gamma = 0.8.$ The pile top seismic masses were lumped at the pile top node. The finite element mesh used for the analysis of Test #2 piles is shown in Figure 4.2. The recorders were placed on the same instrumentation locations as in Test #2.

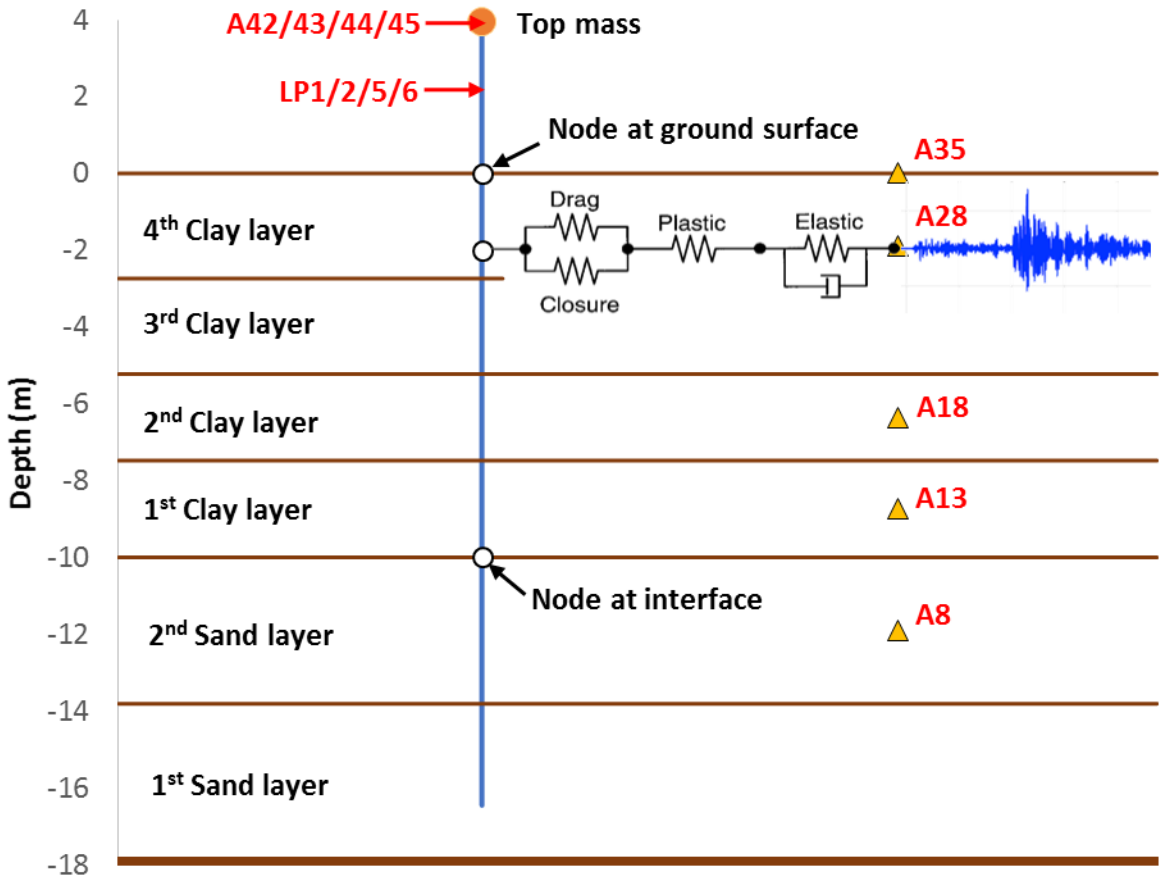

Figure 4.2 Schematic illustration of DYPAC finite element model

4.3 Details of Boulanger et al. (1999) *p-y* Curve

It is important to carefully account for soil-pile yielding, gapping, radiation damping, and soil cave-in and recompression when the BNWF models are applied to problems involving cyclic and dynamic loading (Boulanger et al., 1999; Gerolymos and Gazetas, 2005; Allotey and El Naggar, 2008a and 2008b; Soltani and Muraleetharan, 2018). Incorporating these factors into the non-linear *p-y* elements is a very complex and challenging task even when the soil system is homogeneous.

The history of BNWF methods are discussed in Section 2.1. Among those several *p-y* models, Boulanger el al. (1999) *p-y* curve is a model with input parameters that can be obtained

from in-situ or laboratory tests. This is used as a preliminary model due to its ability to capture the seismic soil structure interaction satisfactorily.

The non-linear *p-y* element proposed by Boulanger et al. (1999) includes elastic (p-y^e), plastic (p-y^p), and gap (p-y^g) elements in series. The elastic component simulates the far-field behavior and a dashpot is connected with elastic spring in parallel to account for the radiation damping in the soil. The plastic component models the near-field behavior of the soil during the seismic event. The gap component includes a non-linear closure spring (p^c-y^g) and a non-linear drag spring (p^d-y^g) connected in parallel in order to simulate the gap opening and closing behavior of soil during the seismic event. The load-deformation behavior of the Boulanger et al. (1999) *p-y* spring components are illustrated in Figure 2.2 in Section 2.1. The values of soil resistance (p_{ult}) and displacement at 50% of p_{ult} (y_{50}) must be specified to define the Boulanger et al. (1999) *p-y* behavior. The popular curves proposed by American Petroleum Institute (API) (‘‘Recommended’’ 1987), and Matlock (1970) were used for sand and clay, respectively to specify the p_{ult} and y_{50} values. These traditional, backbone curves were generated using the built-in models available in LPILE under static loading. Other input parameters recommended by Boulanger et al. (1999) are listed in Table 4-2.

Table 4-2 Input parameters of dynamic *p-y* curve (from Boulanger et al., 1999)

Parameters	Description	Values used in DYPAC	
		Soft clay	Sand
	Soil type	**1**	**2**
Model parameters for plastic spring			
c	Constant to control the tangent modulus at the start of plastic yielding	10	0.5
n	Exponent to control sharpness of p-y^p curve	5	2
c_r	Ratio of p/p_{ult} when plastic yielding first occurs in virgin loading	0.35	0.2
Model parameters for drag spring			
c_d	Ratio of the maximum drag force to the ultimate resistance of the *p-y* element	0.1	0.3

The plastic component shows a rigid behavior initially in the range between $\pm c_r p_{ult}$. Then the rigid behavior translates into plastic yielding. The behavior of the closure spring does not depend on any other input parameters other than previous gap opening and closing memory terms for the positive and negative gap spring displacements. Note that some of the input parameters for Boulanger et al. (1999) *p-y* model (p_{ult} and y_{50}) were based on the backbone curves that were generated in LPILE program.

In DYPAC, the code section to model the *p-y* response was obtained and modified from the open-source available in Github that was originally developed by Boulanger for OpenSees, sponsored by the Pacific Earthquake Engineering Research Center (URL https://github.com/lge88/OpenSees/blob/master/SRC/material/uniaxial/PY/PySimple1.cpp).

4.4 Site Response Analyses

4.4.1 DEEPSOIL Modeling

Equivalent Linear (EL) analyses were performed for a level ground using the computer program called DEEPSOIL (Hashash et al., 2016). The EL model engages an iterative method in determining the shear modulus and damping ratio of the given soil properties that is similar to the program SHAKE2000 (Ordonez, 2012). Soil properties are input using discrete points to simulate the backbone curve. The G/G_{max} and the damping ratio (%) curves are defined as functions of shear strain (%). These curves for clay and sand were modeled using San Francisco Bay Mud curves provided by Stokoe and Lodde (1978) and square root-relative method for granular soils proposed by Seed and Idriss (1970), respectively. Figure 4.3 shows the curves used in DEEPSOIL modeling. The San Francisco Bay Mud is also a soft clay and is considered a reasonable representation of the soft clay modeled here.

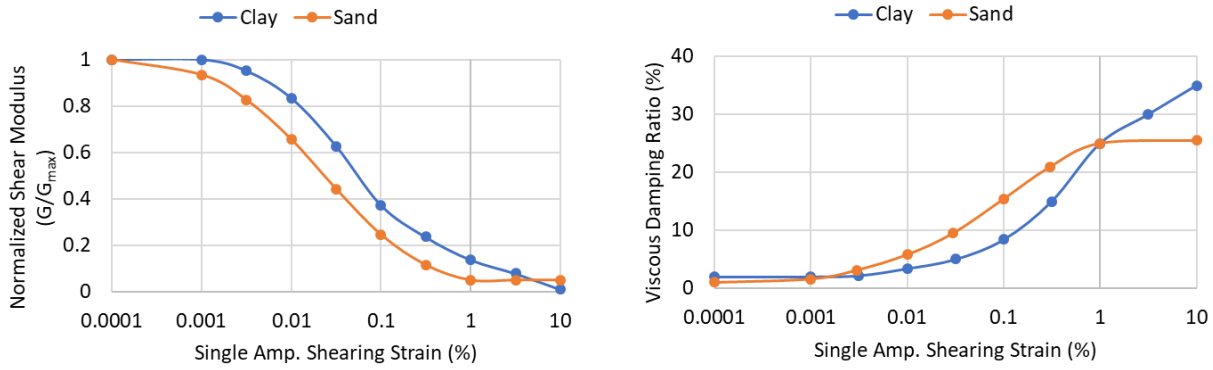

Figure 4.3 G/G_{max} and damping curves used in DEEPSOIL modeling

Dickenson (1994) proposed the empirical relationship for the shear velocity (v_s) for cohesive soils in the San Francisco Bay Area. The relationship is given by $v_s = 18(s_u)^{0.475}$ and this equation is used to calculate the shear velocity of soft clay where s_u is the undrained shear

strength. The average shear wave velocity of the sand layer was taken as 482 m/s as calculated in Taghavi (2017), using the empirical equation provided by Seed and Idriss (1970).

4.4.2 Free-field Soil Displacements

Three base motion events were applied to the centrifuge model. The first two events were scaled versions of a motion recorded in 1989 in California during the Loma Prieta earthquake, and the third event was a scaled version of a motion recorded in 1995 in Japan during the Kobe earthquake. Figure 4.4 shows the base motion acceleration time histories recorded during Test #2. These base motion time histories were applied in DEEPSOIL analyses.

In the centrifuge tests, soil displacements were obtained by double integrating acceleration-time histories recorded in the far-field. The back-calculated maximum displacements at the soil surface were 2 cm, 4 cm, and 25 cm for the first, second, and third events, respectively (Soltani, 2016). The DEEPSOIL analyses predicted them as 2.5 cm, 5 cm, and 35 cm, respectively. Figure 4.5 shows the soil displacements obtained using DEEPSOIL for Events 1, 2, and 3. Note that the quality of soil displacements obtained from DEEPSOIL will impact the pile responses predicted by DYPAC. For Event 1, the far-field acceleration predictions are compared with the recorded values as shown in Figure 4.6. The locations of free-field accelerometers are shown in Figure 4.2. The predictions and recorded acceleration-time histories show a reasonable agreement in terms of trend, peak locations and magnitudes. For Event 2 and 3, the comparisons between DEEPSOIL-predicted and recorded far-field accelerations were similar and had reasonable agreement in terms of trend, peak locations and magnitudes. Therefore, those comparisons are not shown here.

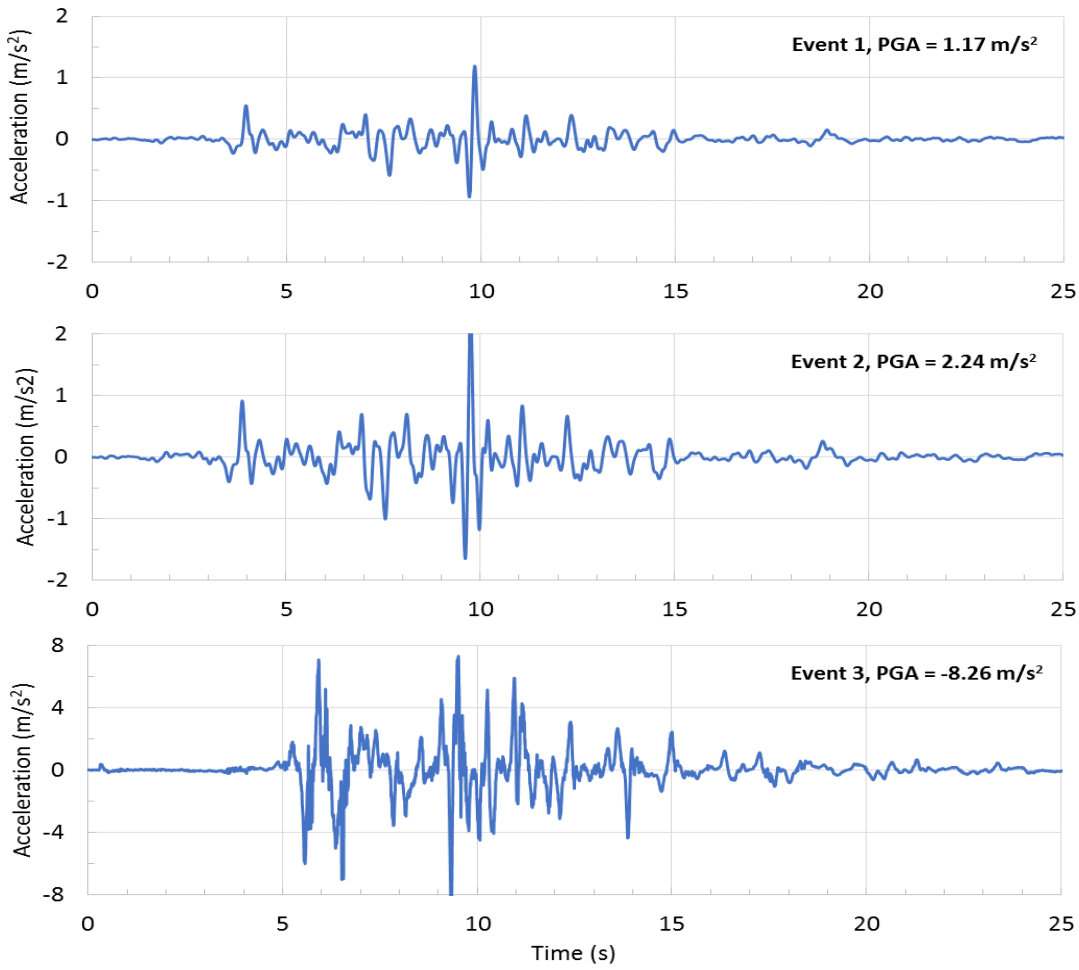

Figure 4.4 Base-motion acceleration-time histories recorded in Events 1, 2, and 3

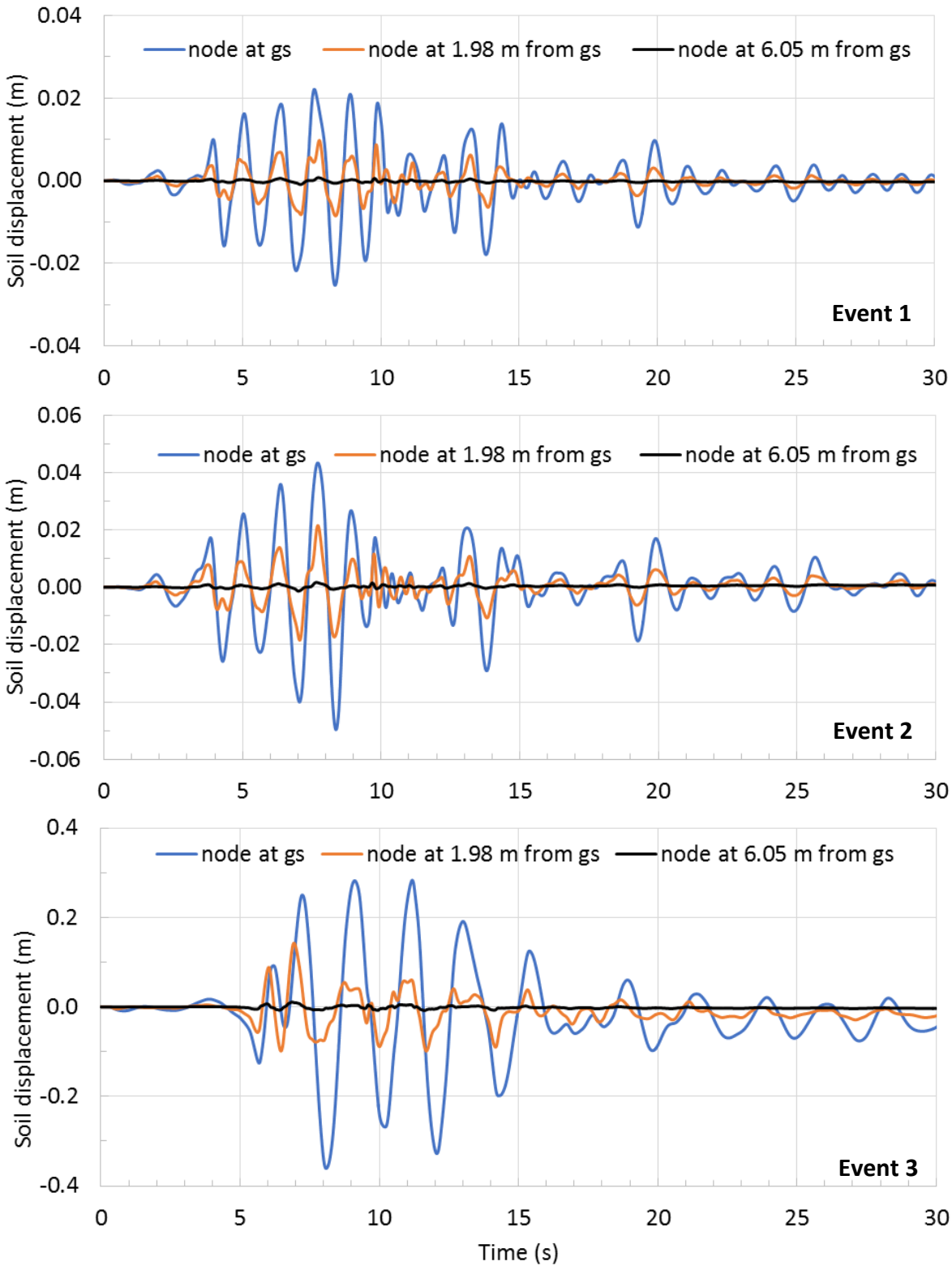

Figure 4.5 Soil displacement-time histories predicted by DEEPSOIL for Events 1, 2, and 3

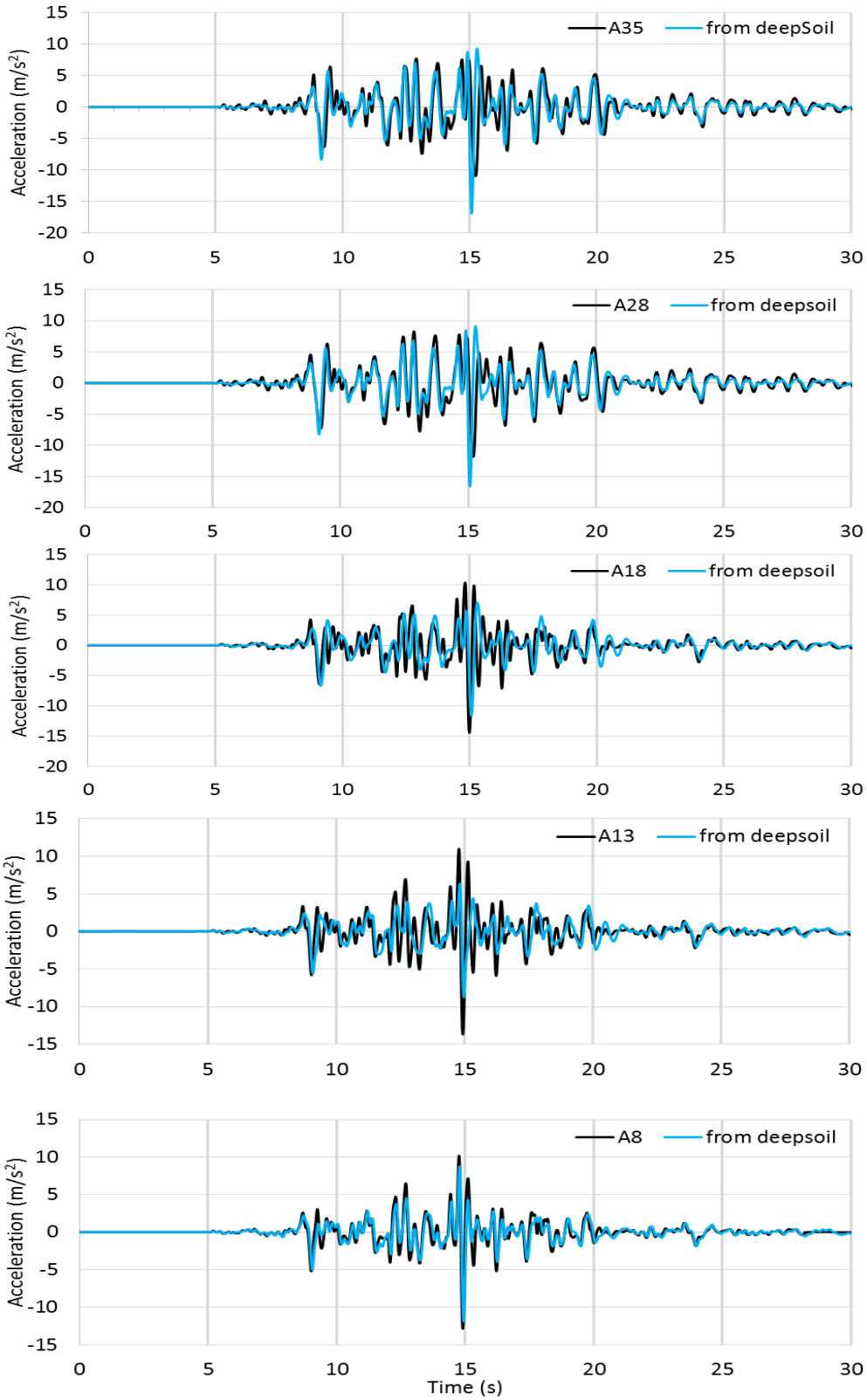

Figure 4.6 Acceleration-time histories recorded by the far-field accelerometers and predicted by DEEPSOIL

4.5 Comparisons between DYPAC Predictions and Centrifuge Test Results

The free-field soil displacements obtained using DEEPSOIL analyses were applied in DYPAC and the pile deflections, accelerations, and bending moments were predicted both in unimproved and improved soils. The CDSM improved soil was modeled in DYPAC using the proposed method explained in Section 3.5. The locations of displacement transducers (Linear potentiometer - LP), accelerometers (A), and strain gauges are shown in Figures 4.1 and 4.2. In the following sections and plots, the piles in unimproved soil are denoted by UIAB, the piles with improved depths of 6D, 9D, and 12D are denoted by 6DEF, 9DIJ, and 12DMN, respectively (see Figure 4.1). For Event 3, the pile 12DMN had convergence issues after 12 seconds therefore, those results are plotted only till 12 seconds. The analysis of the pile 12DMN for Event 3 will be carried out using smaller time steps.

4.5.1 Pile Deflections

For comparison purposes, the DYPAC-predicted lateral pile deflections were obtained at two nodes on the free length of the pile outside the soil. These time histories are compared with the measured values obtained from a displacement transducer outside the soil and from values obtained by double integrating the acceleration-time histories obtained from the accelerometers placed on the seismic masses on pile top (see Figure 4.2 for these locations). Figures 4.7 through 4.9 compare the DYPAC-predicted and measured displacement-time histories. The measured displacement-time histories represent the pile displacements relative to the centrifuge container base. This is comparable with the relative pile displacements (y_{rp}, see Section 2.2) predicted by DYPAC.

The maximum displacements measured by displacement transducers were 4 cm, 4.5 cm, and 60 cm for Events 1, 2, and 3, respectively. DYPAC predicted them as 6 cm, 8 cm, and 80 cm, respectively. These predicted displacements are larger than the measured values. One possible reason for this discrepancy may be the neglected pile damping. Further, DYPAC-predicted displacement-time histories exhibited larger frequencies compared to the ones measured by the displacement transducers. The displacement transducers used in these tests are known to under estimate the frequency of the displacements during the seismic testing in the centrifuge and this is likely the reason for the above mentioned discrepancy.

The DYPAC-predicted and measured displacement-time histories for all cases and for all events are summarized in Figures 4.10 and 4.11, respectively. Overall DYPAC predictions show that the UIAB has the largest displacements in all three shaking events, whereas 6DEF has the second largest, and 9DIJ and 12DMN have smaller and similar displacement-time histories. Conversely, the measured values (see Figure 4.11) show that the 6DEF has the largest and UIAB has the second largest displacement. However, the measured values were smaller and similar for 9DIJ and 12DMN, and this implies that 9D improvement was sufficient to reduce the pile displacements (Soltani, 2016).

4.5.2 Pile Top Accelerations

DYPAC-predicted acceleration-time histories are compared with the measured values obtained from the accelerometers placed on the seismic masses at the pile top. The accelerometers recorded the absolute accelerations. Therefore in DYPAC, the base motion accelerations ($\ddot{u}_g$) were added to the relative accelerations ($\ddot{y}_{rp}$) to obtain the absolute values. The predicted accelerations on nodes were noisy and exhibited high frequencies. Therefore, the nodal

acceleration values were averaged for an element. For pile top acceleration values, the average value for pile element including pile top node is considered. Similar high frequency and noisy acceleration-time histories were also observed in the computer code (DYSAC2) and the accelerations were averaged for an element (Muraleetharan et al., 1988, 1997b).

The predicted and measured accelerations for Event 1 and Event 2 are plotted in Figures 4.12 and 4.13, respectively. These predicted accelerations are an order of magnitude higher than the measured values. The maximum accelerations recorded by pile top accelerometers were 1.2 m/s^2 and 2.4 m/s^2 for Events 1 and 2, respectively. DYPAC predicted them as 10 m/s^2 and 20 m/s^2, respectively. For Event 3, these values were significantly higher and noisier, than for Events 1 and 2 and are not shown here. The exact reasons for these discrepancies are still being investigated.

4.5.3 Bending Moments

DYPAC-predicted bending moment-time histories are plotted in Figures 4.14 through 4.27 for piles UIAB, 6DEF, 9DIJ and 12DMN and for all shaking events. In DYPAC, the bending moments and shear forces are obtained by multiplying the stiffness matrix by the displacement vector. Due to malfunction of data acquisition system, the bending moment histories were not obtained in the centrifuge tests for piles UIAB, 6DEF, and 9DIJ in the first and second events.

The bending moment data derived from stain gauge for the pile in 12DMN in Events 1, 2, and 3 are compared with the DYPAC-predicted bending moment-time histories in Figures 4.17, 4.21, and 4.27, respectively. Figures 4.23 and 4.24 shows the DYPAC-predicted and measured bending moment-time histories for UIAB and 6DEF in Event 3. It can be seen, from the

available measured data, that the DYPAC-predicted bending moments have same order of magnitude and trend as measured values.

The measured peak bending moments were 60 kN.m, 60 kN.m, and 350 kN.m for Events 1, 2, and 3, respectively, and all of them occurred in piles in 12DMN. DYPAC-predicted peak bending moments were 60 kN.m, 70 kN.m, and 450 kN.m for Events 1, 2, and 3, respectively. For Events 1 and 2, the largest bending moment prediction occurred in piles in 9DIJ and 12DMN (similar trend in time histories), the second largest occurred in 6DEF and the smallest one was in UIAB. This was inconsistent with the fact that the larger improvements result in higher bending moments, and after 9D improvement, the effect of improvement was not significant; therefore, 9DIJ and 12DMN predicted similar time histories. Conversely in Event 3, the bending moments were slightly larger in 12DMN than 9DIJ. Overall, the predicted and measured bending moment values along the length of the pile show reasonable agreement.

4.6 Summary of Observations and Conclusions

- The DYPAC-predicted displacements are in same order as the measured values and overall, the predicted displacement follows the similar trend as the measured values. However, the predicted displacement magnitudes were slightly higher compared to the measured values.

- Overall the predicted bending moment values were in good agreement with the measured bending moments.

- Conversely, the pile acceleration predictions were higher by an order of magnitude and the time histories were noisy compared to the measured results. The exact reasons for

these discrepancies are still being investigated.

Note that the quality of free-field soil displacements obtained from DEEPSOIL impacts the pile responses predicted by DYPAC. DYPAC predictions are expected to improve if non-linear analyses using computer codes such as DYSAC2 (Muraleetharan et al., 1988, 1997b) are used for free-field analyses.

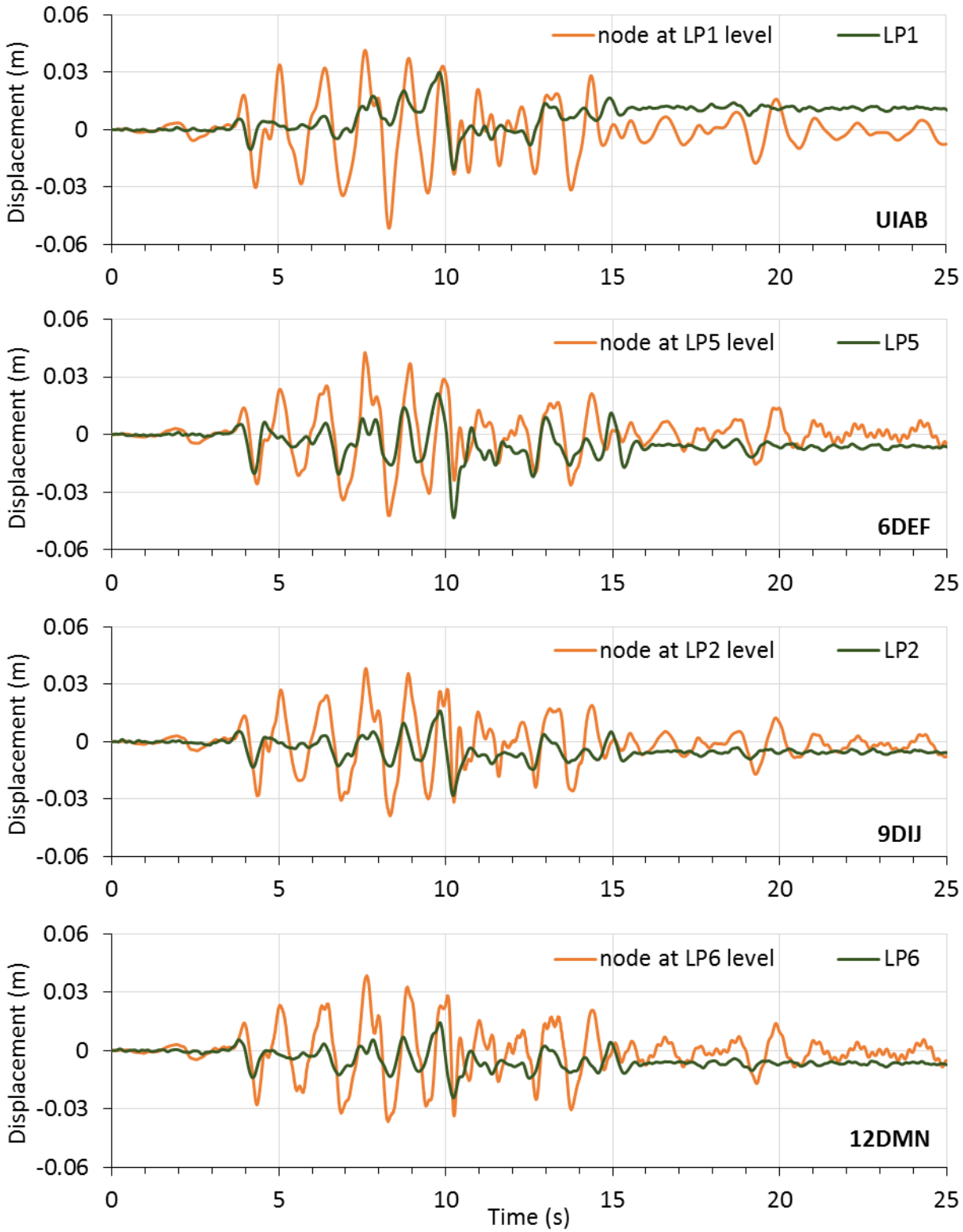

Figure 4.7 Pile displacement-time histories predicted by DYPAC and measured by displacement transducers for Event 1

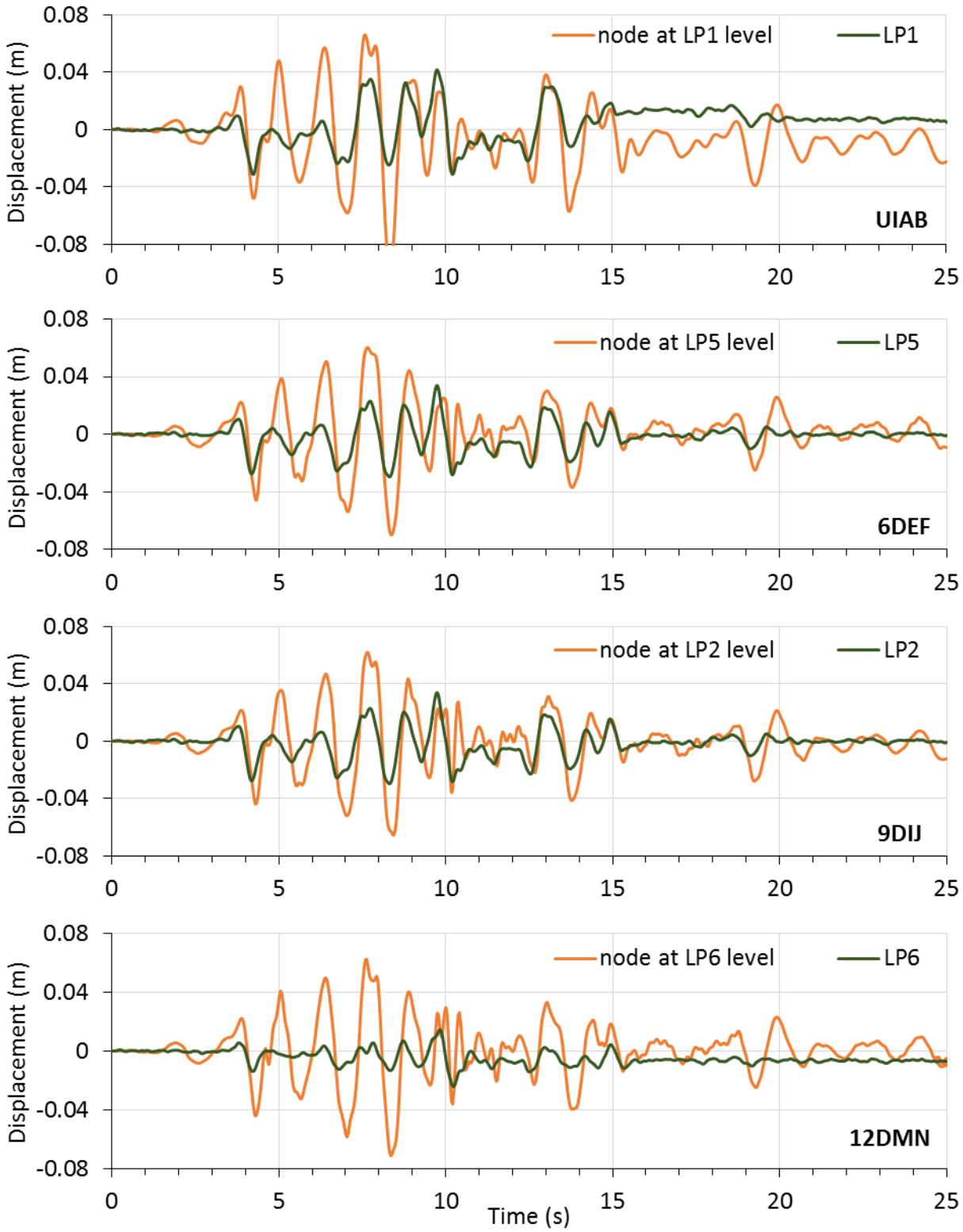

Figure 4.8 Pile displacement-time histories predicted by DYPAC and measured by displacement transducers for Event 2

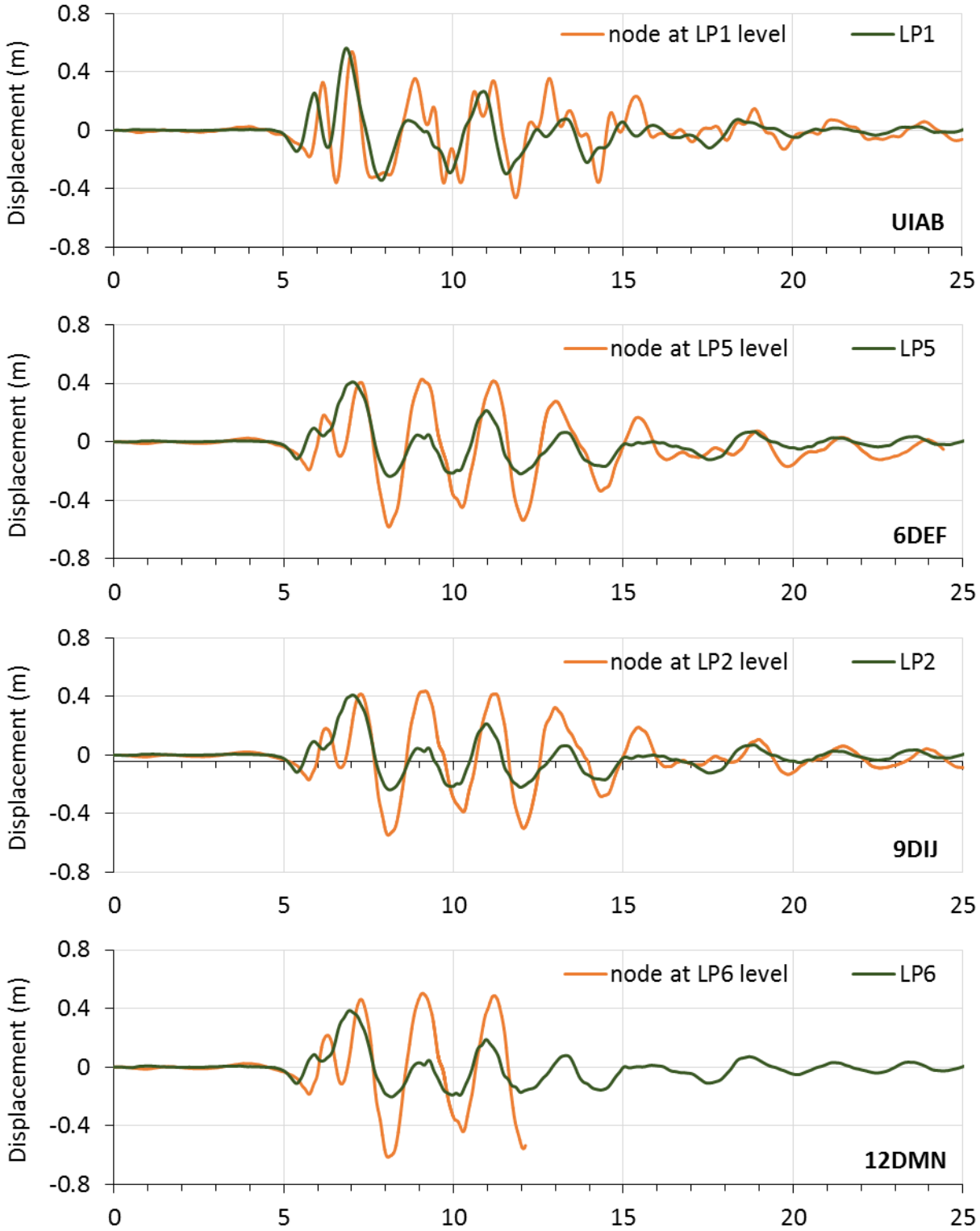

Figure 4.9 Pile displacement-time histories predicted by DYPAC and measured by displacement transducers for Event 3

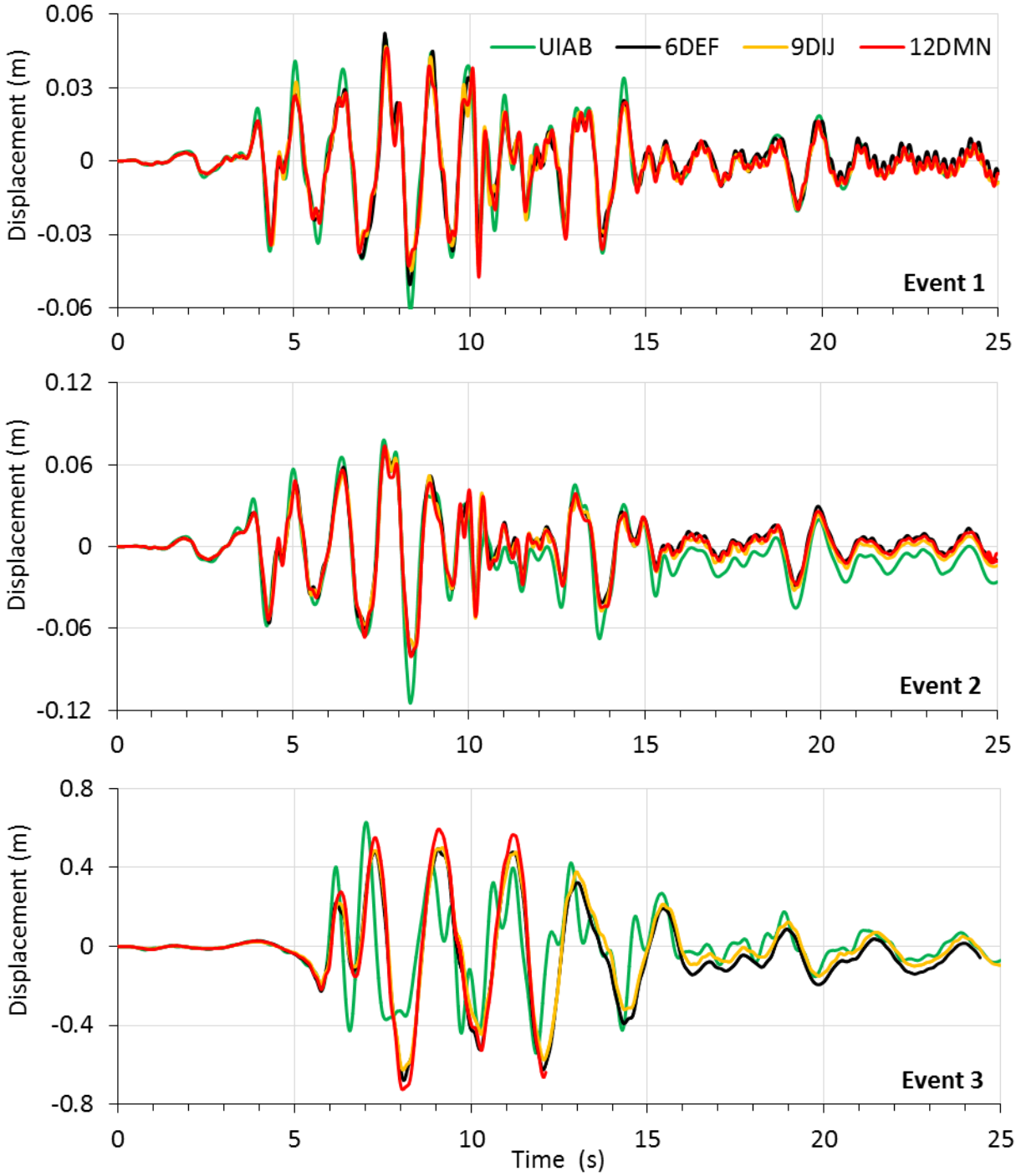

Figure 4.10 Time histories of displacements with respect to base obtained from DYPAC for all shaking events

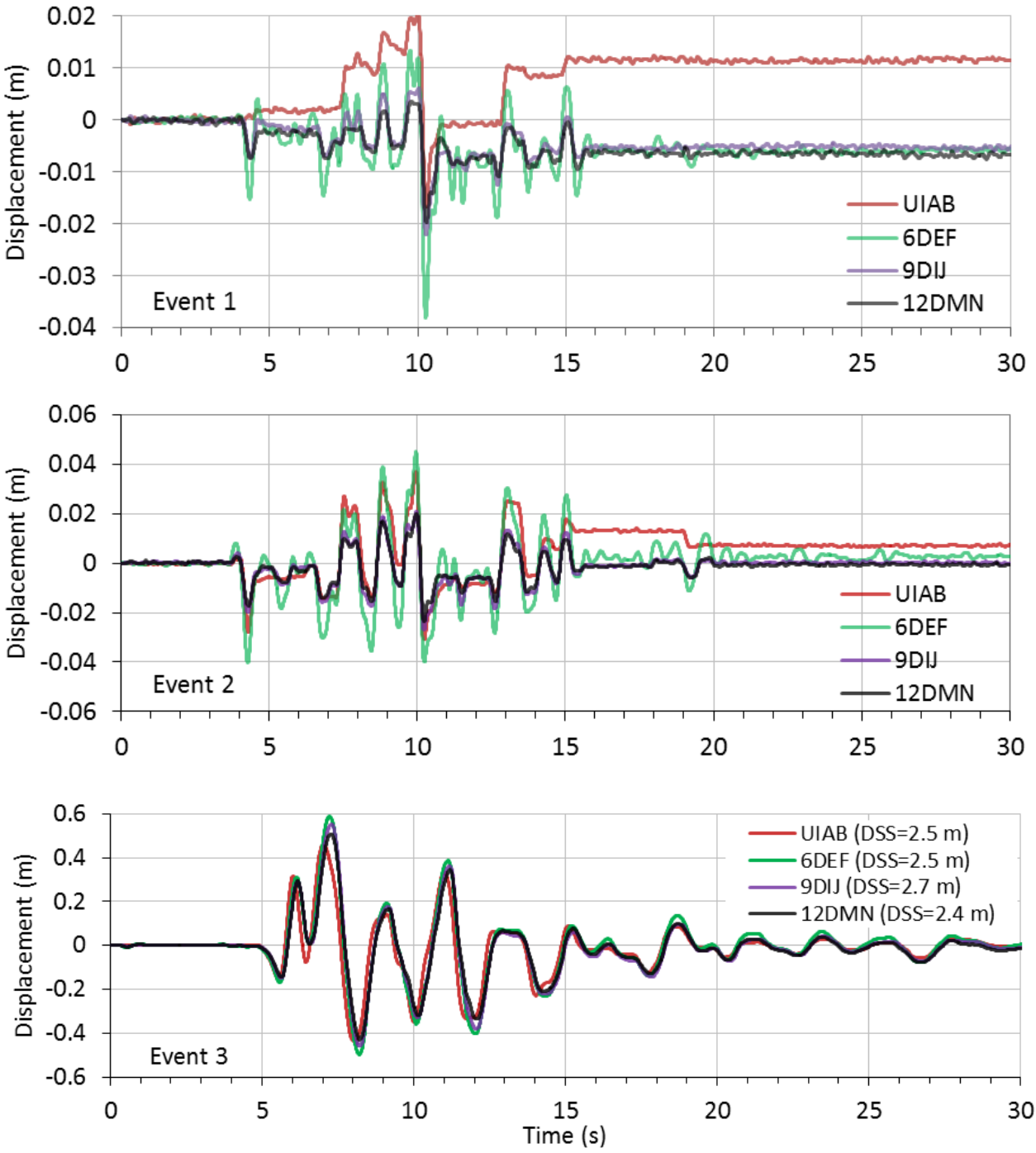

Figure 4.11 Time histories of displacements recorded in transducers in all shaking events (from Soltani, 2016)

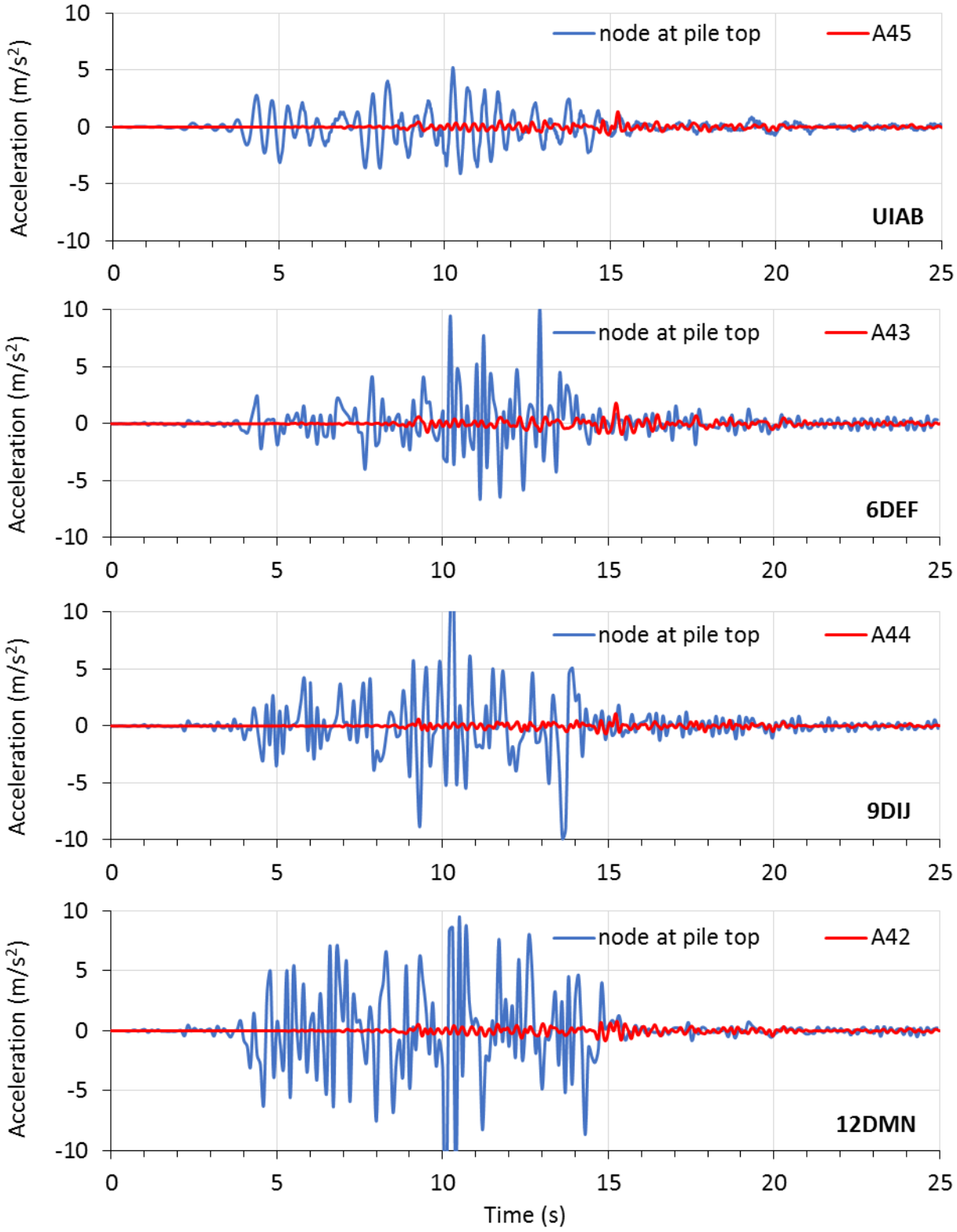

Figure 4.12 Pile acceleration-time histories predicted by DYPAC and measured by top mass accelerometers for Event 1

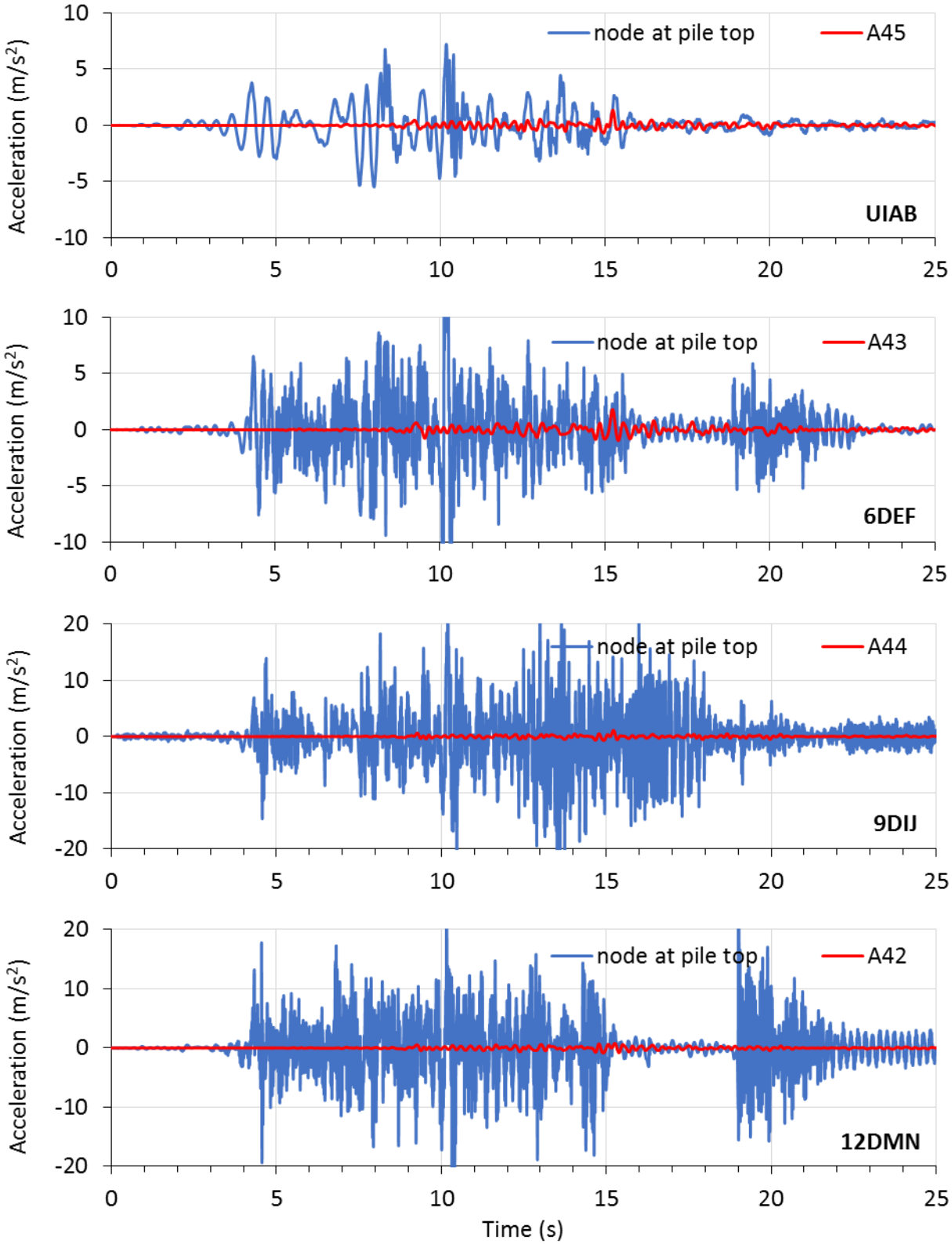

Figure 4.13 Pile acceleration-time histories predicted by DYPAC and measured by top mass accelerometers for Event 2

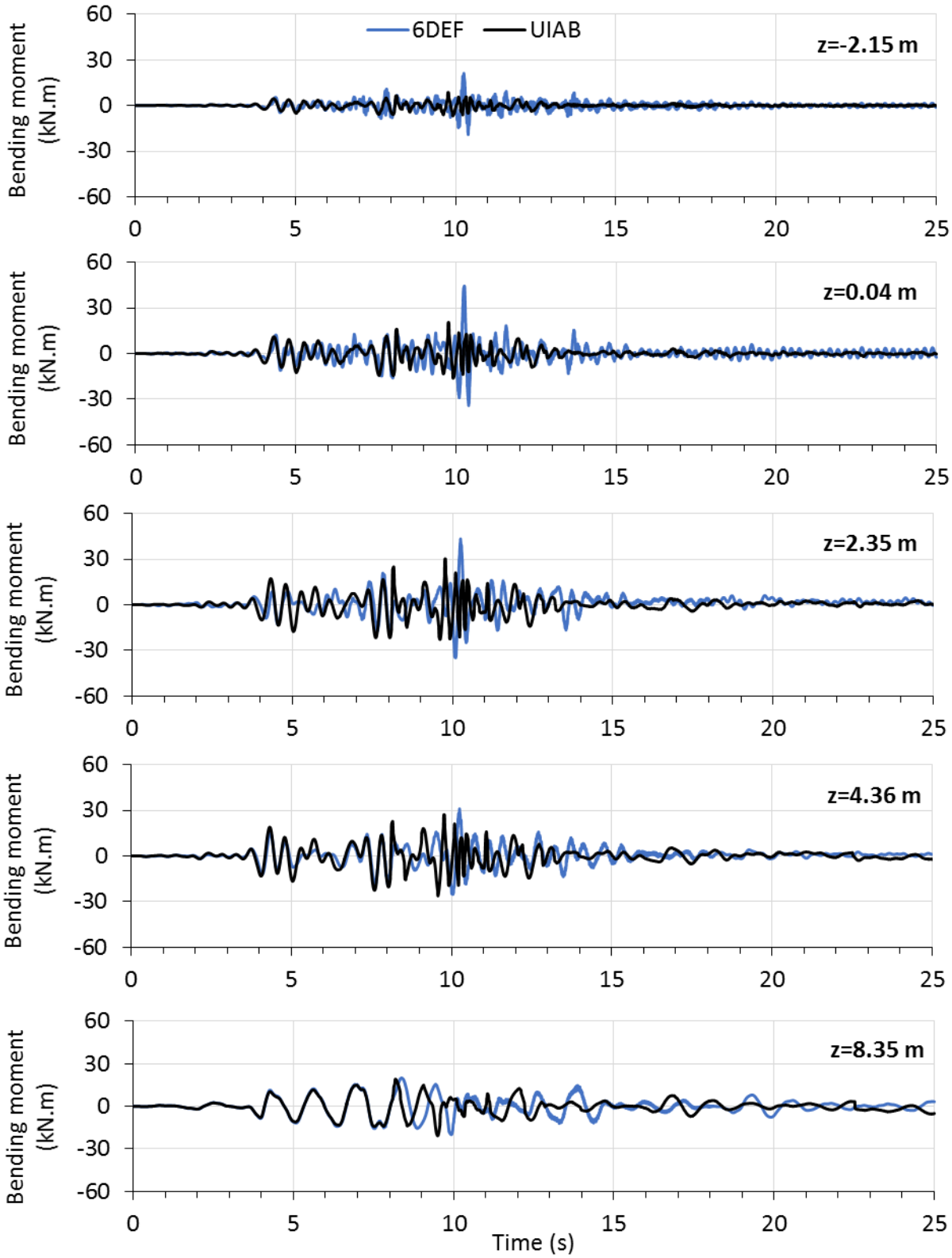

Figure 4.14 Bending moments predicted by DYPAC for UIAB and 6DEF for Event 1 (z is depth from the ground surface; negative values imply above ground.)

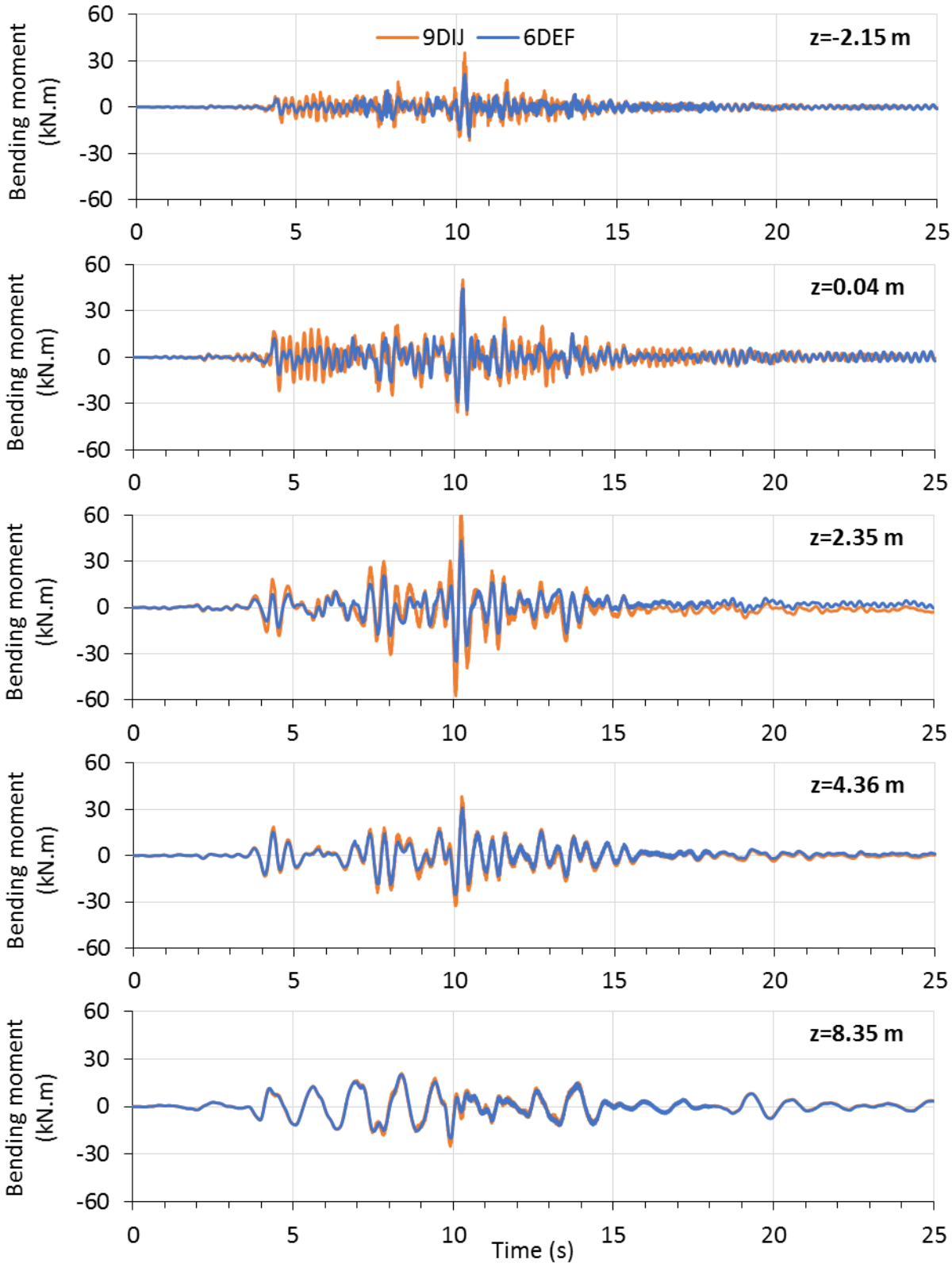

Figure 4.15 Bending moments predicted by DYPAC for 6DEF and 9DIJ for Event 1 (z is depth from the ground surface; negative values imply above ground.)

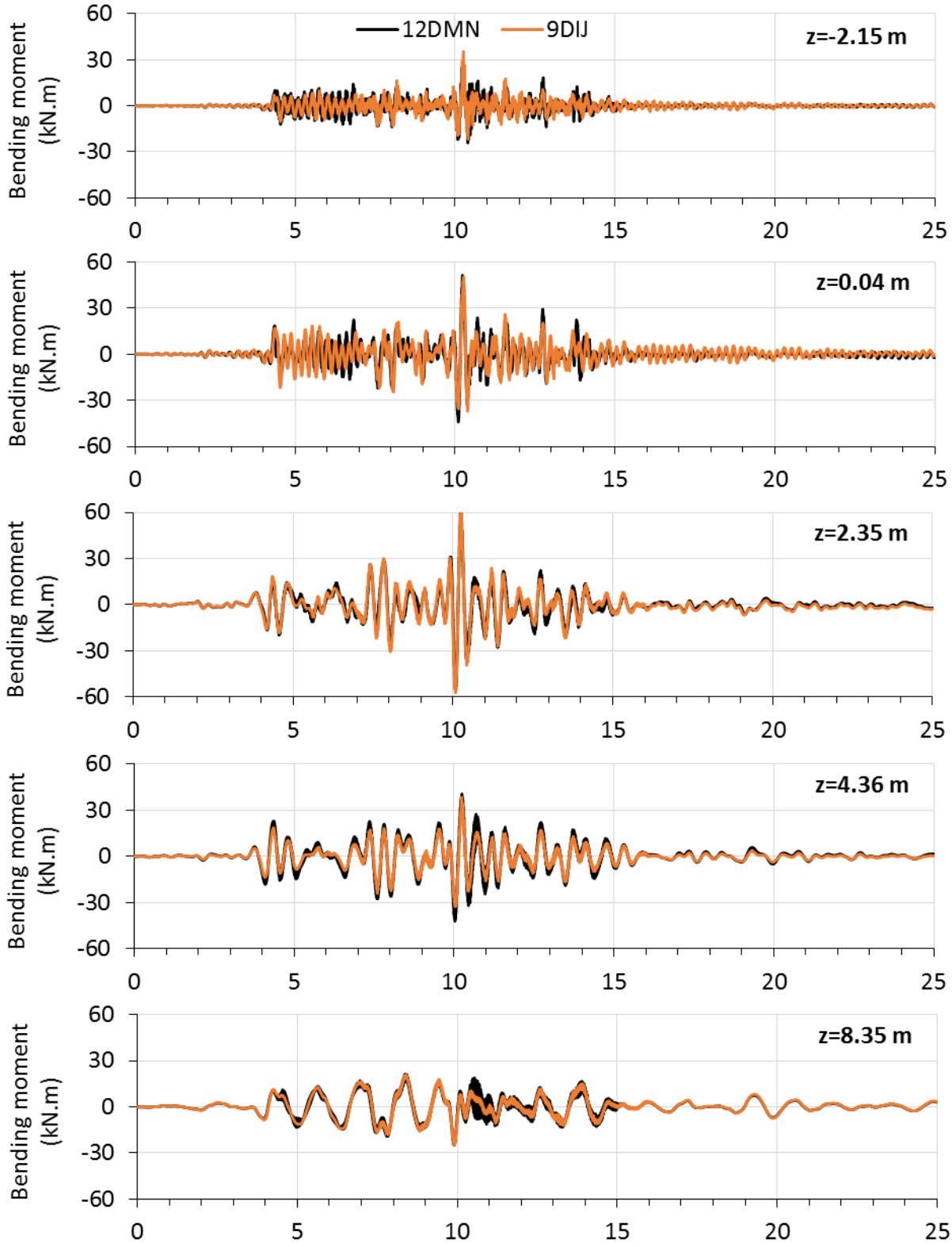

Figure 4.16 Bending moments predicted by DYPAC for 9DIJ and 12DMN for Event 1 (z is depth from the ground surface; negative values implies above ground)

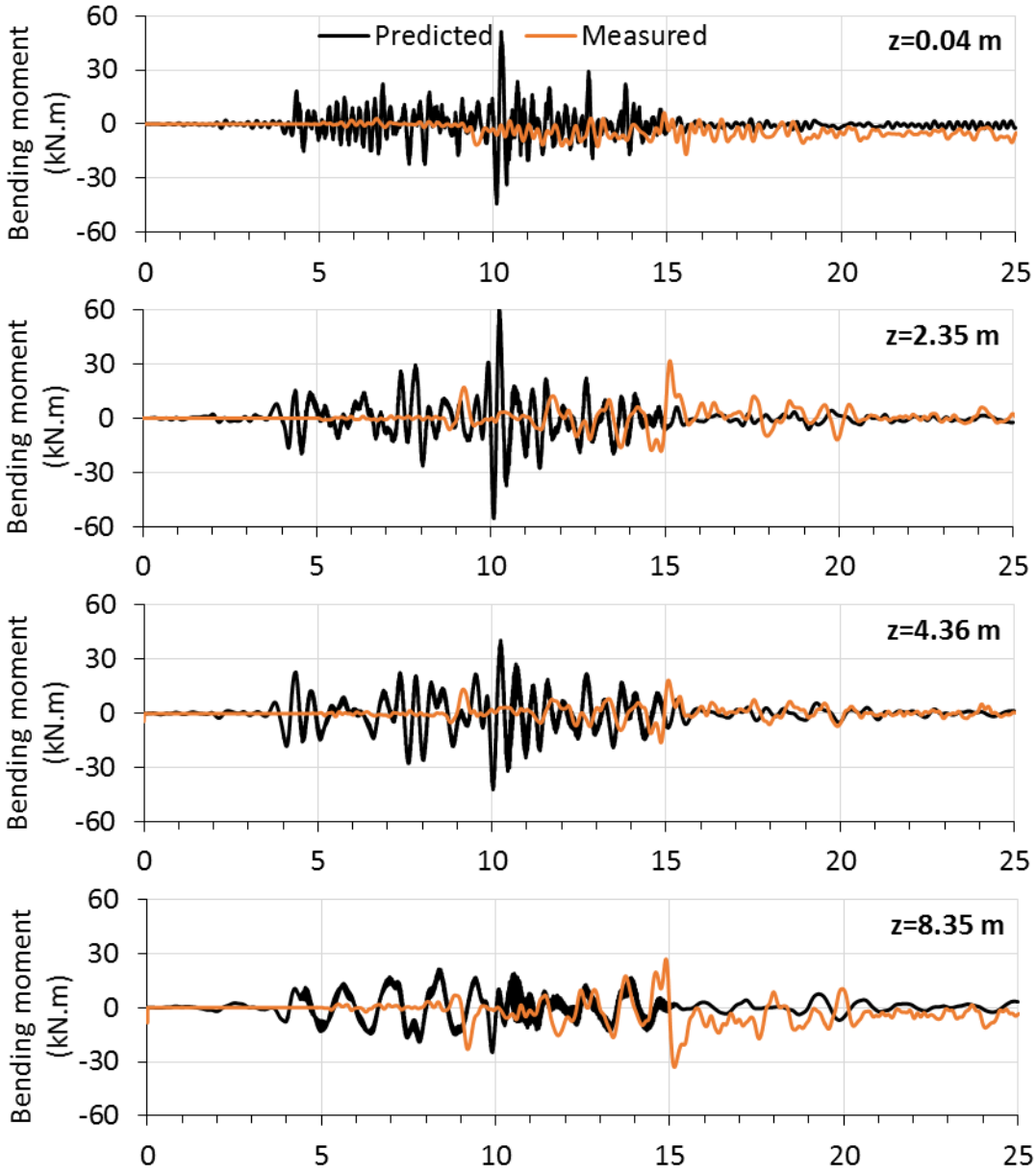

Figure 4.17 DYPAC-predicted and measured bending moment-time histories for 12DMN for Event 1 (z is depth from the ground surface)

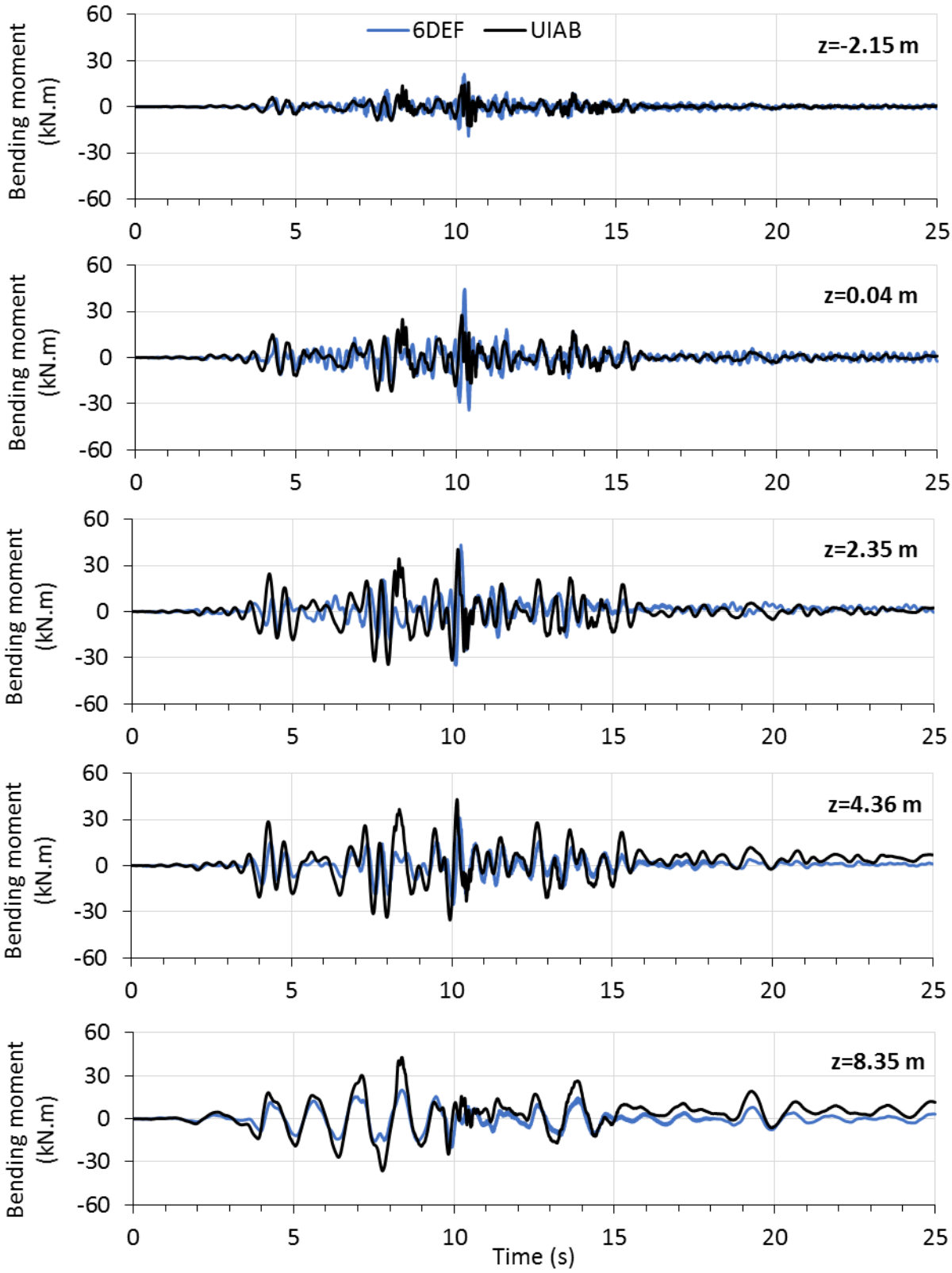

Figure 4.18 Bending moments predicted by DYPAC for UIAB and 6DEF for Event 2 (z is depth from the ground surface; negative values implies above ground)

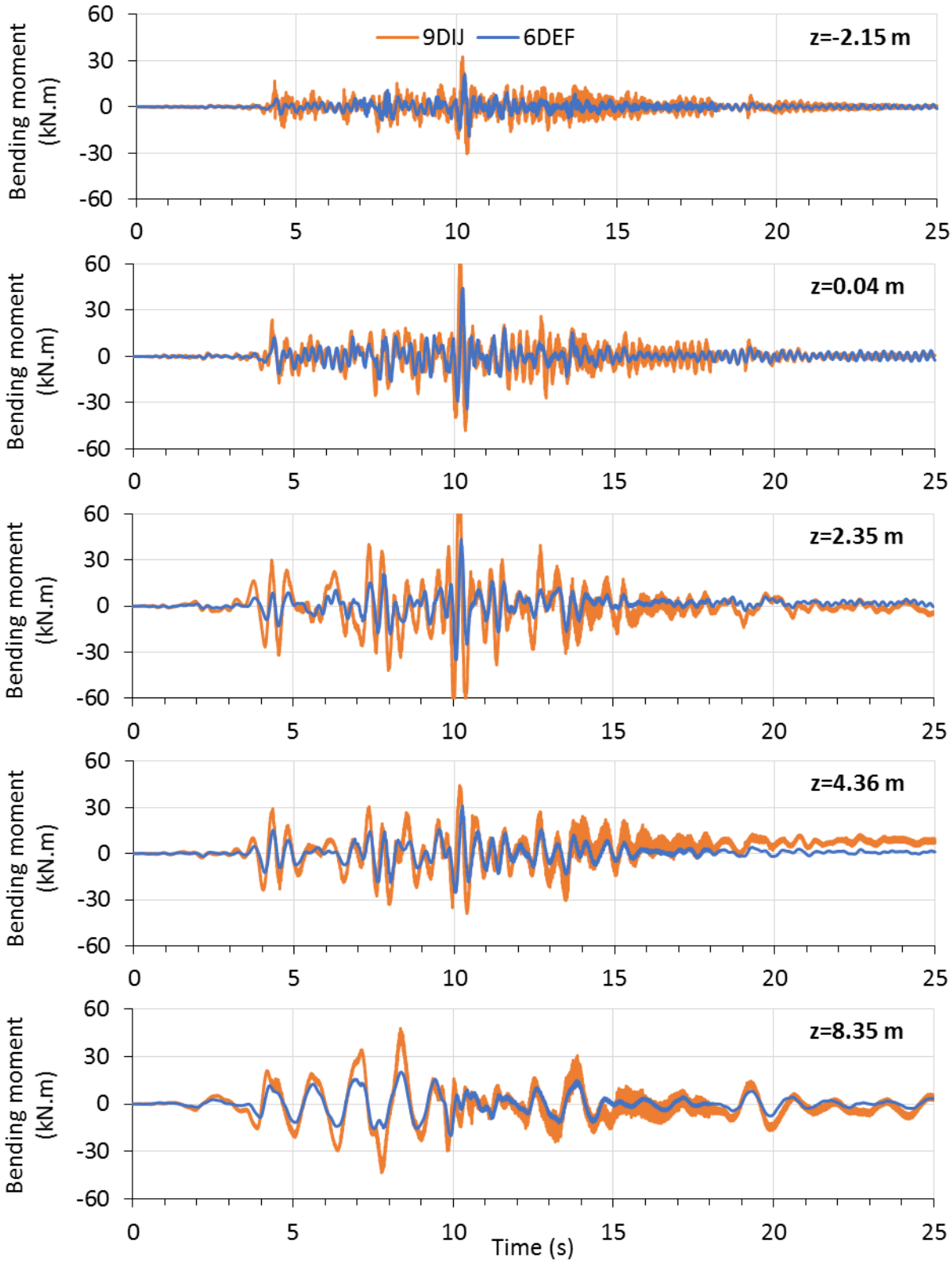

Figure 4.19 Bending moments predicted by DYPAC for 6DEF and 9DIJ for Event 2 (z is depth from the ground surface; negative values implies above ground)

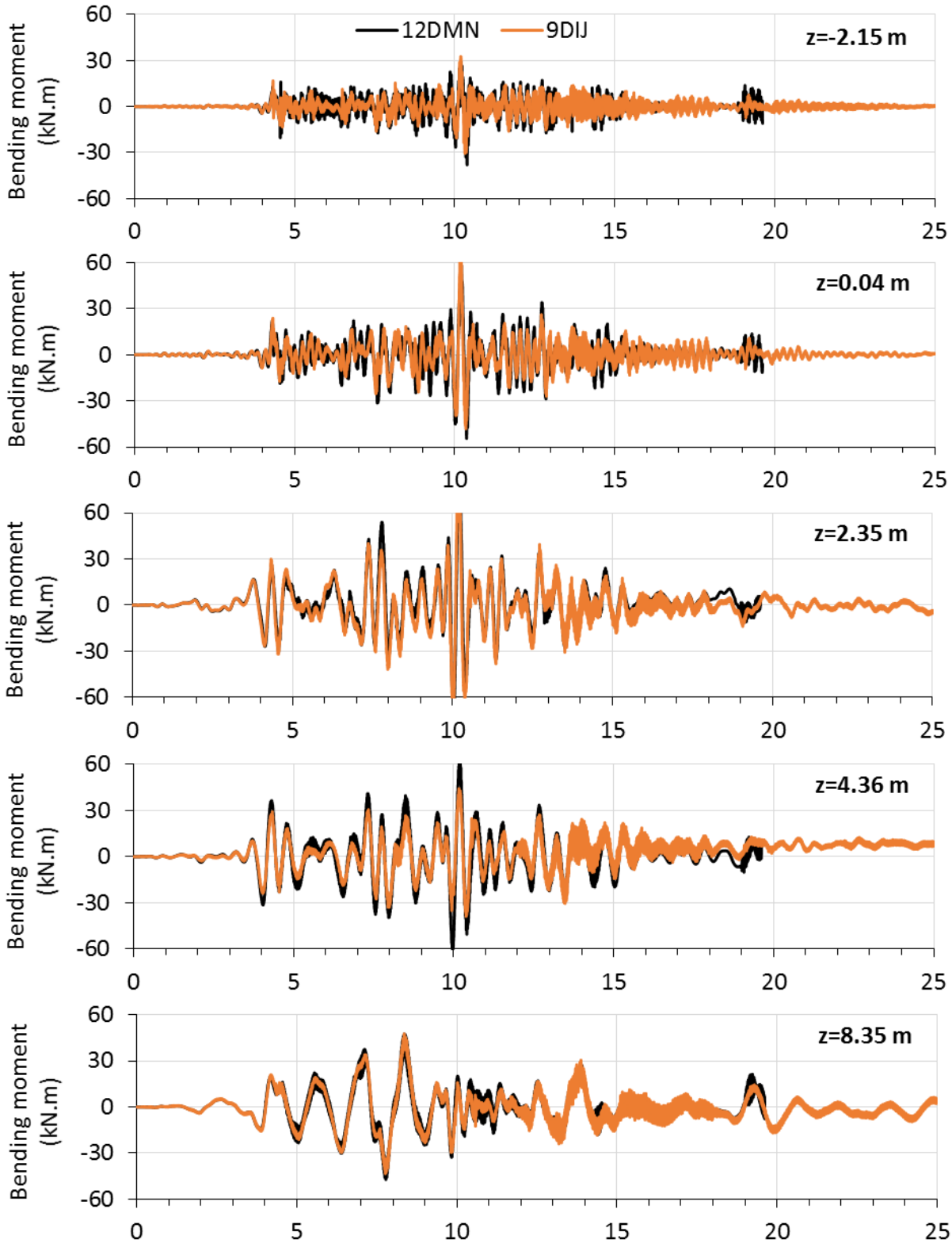

Figure 4.20 Bending moments predicted by DYPAC for 9DIJ and 12DMN for Event 2 (z is depth from the ground surface; negative values implies above ground.)

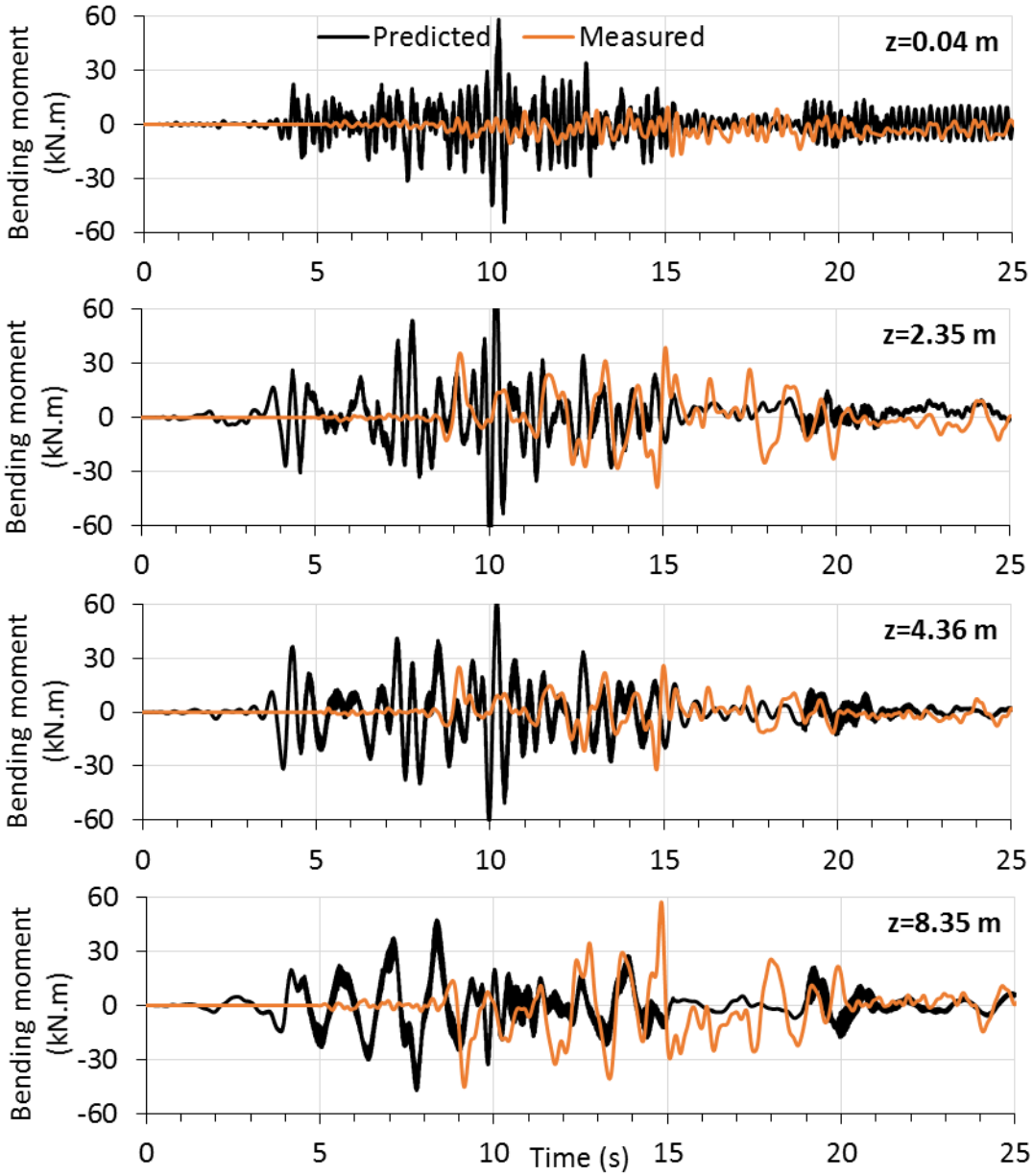

Figure 4.21 DYPAC-predicted and measured bending moment-time histories for 12DMN for Event 2 (z is depth from the ground surface)

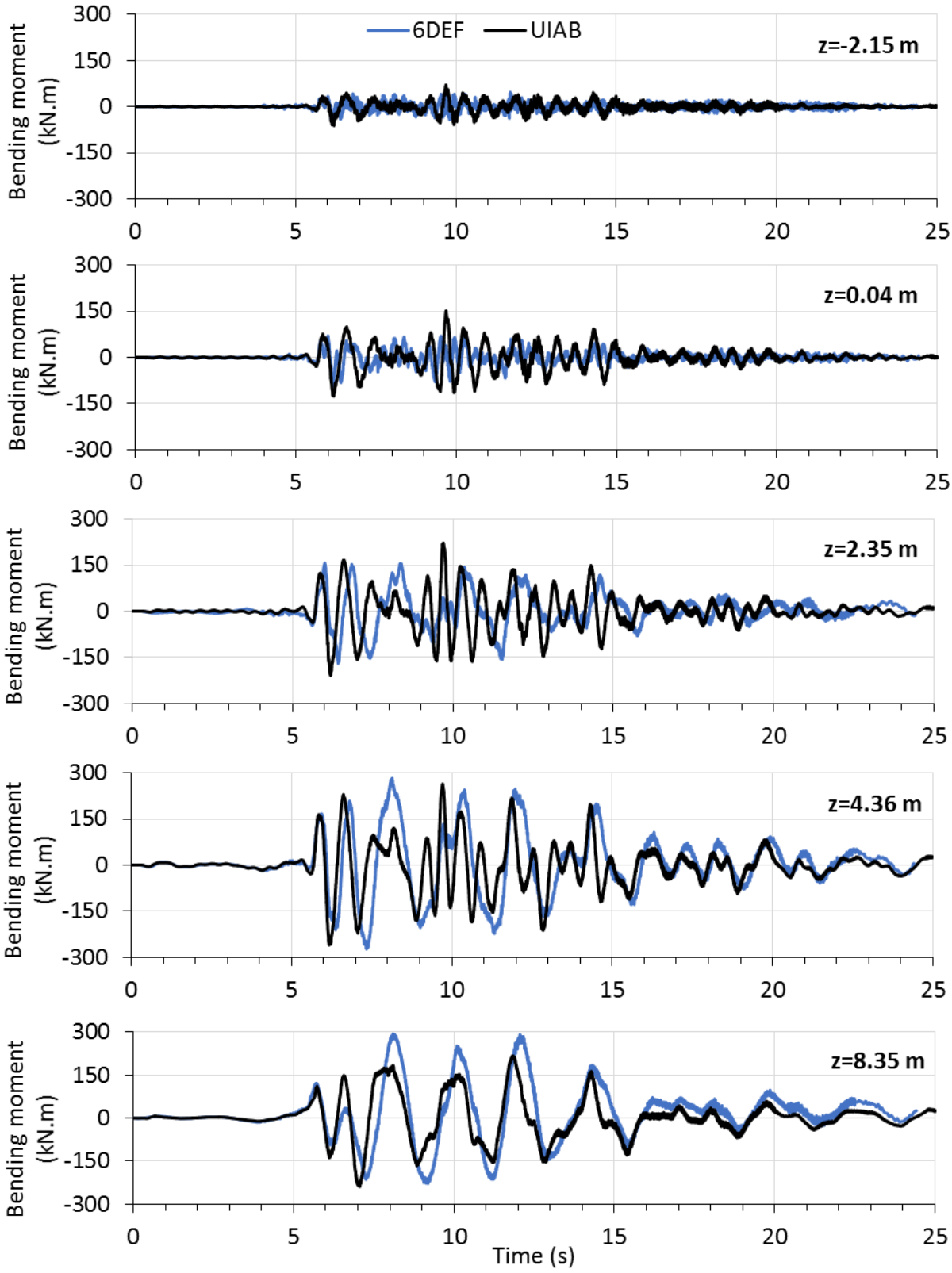

Figure 4.22 Bending moments predicted by DYPAC for UIAB and 6DEF for Event 3 (z is depth from the ground surface; negative values implies above ground.)

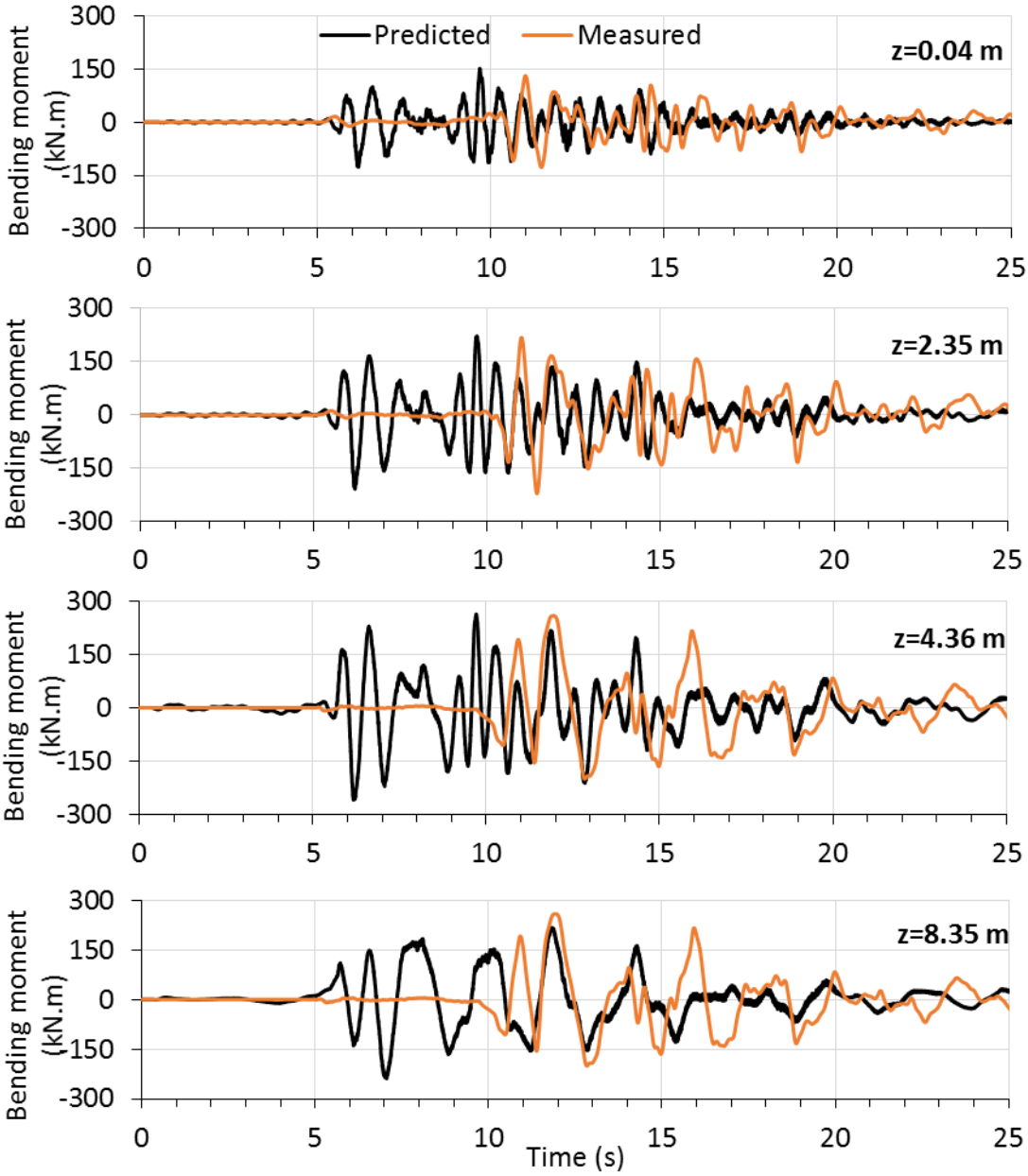

Figure 4.23 DYPAC-predicted and measured bending moment-time histories for UIAB for Event 3 (z is depth from the ground surface)

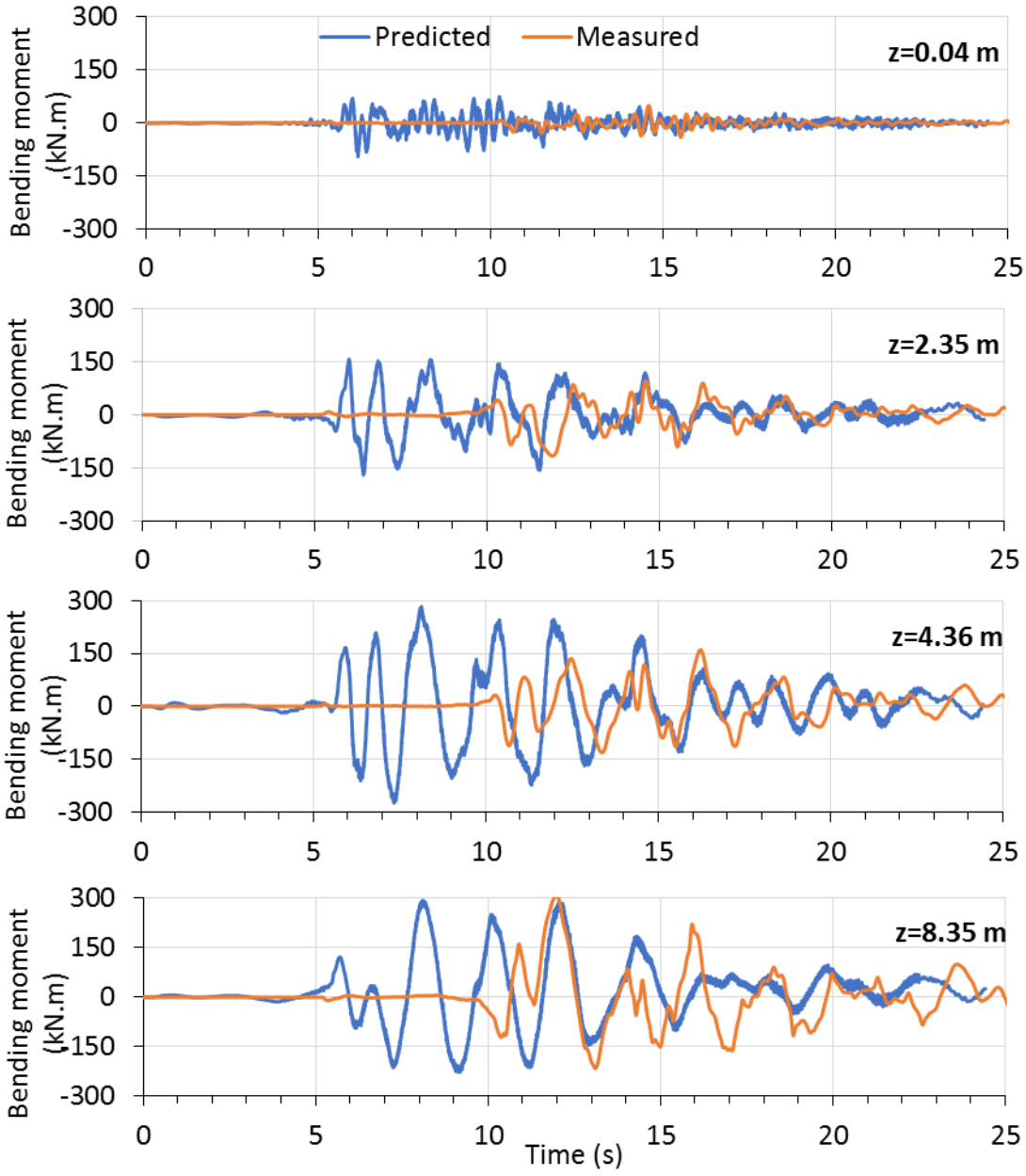

Figure 4.24 DYPAC-predicted and measured bending moment-time histories for 6DEF for Event 3 (z is depth from the ground surface)

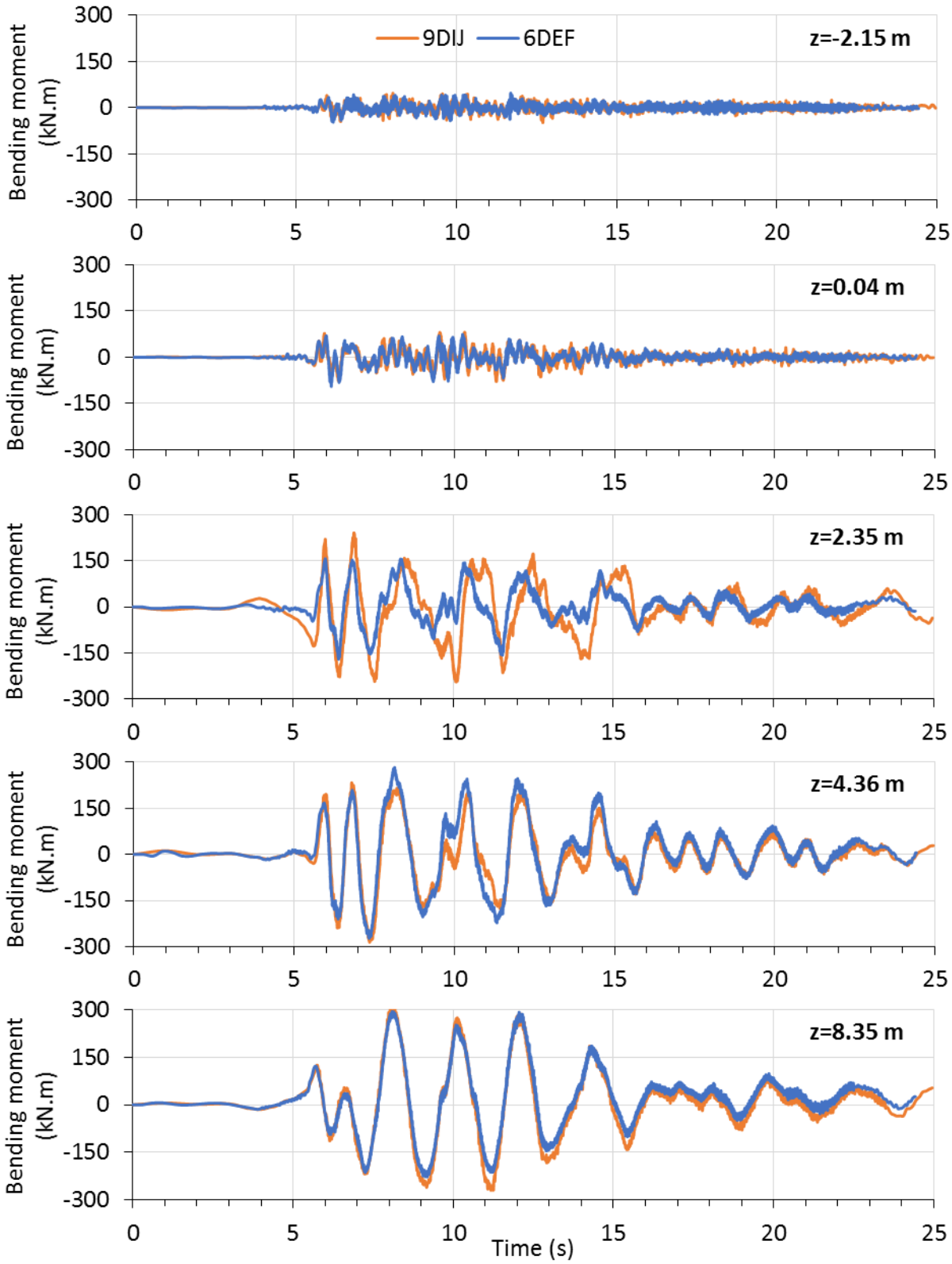

Figure 4.25 Bending moments predicted by DYPAC for 6DEF and 9DIJ for Event 3 (z is depth from the ground surface; negative values implies above ground)

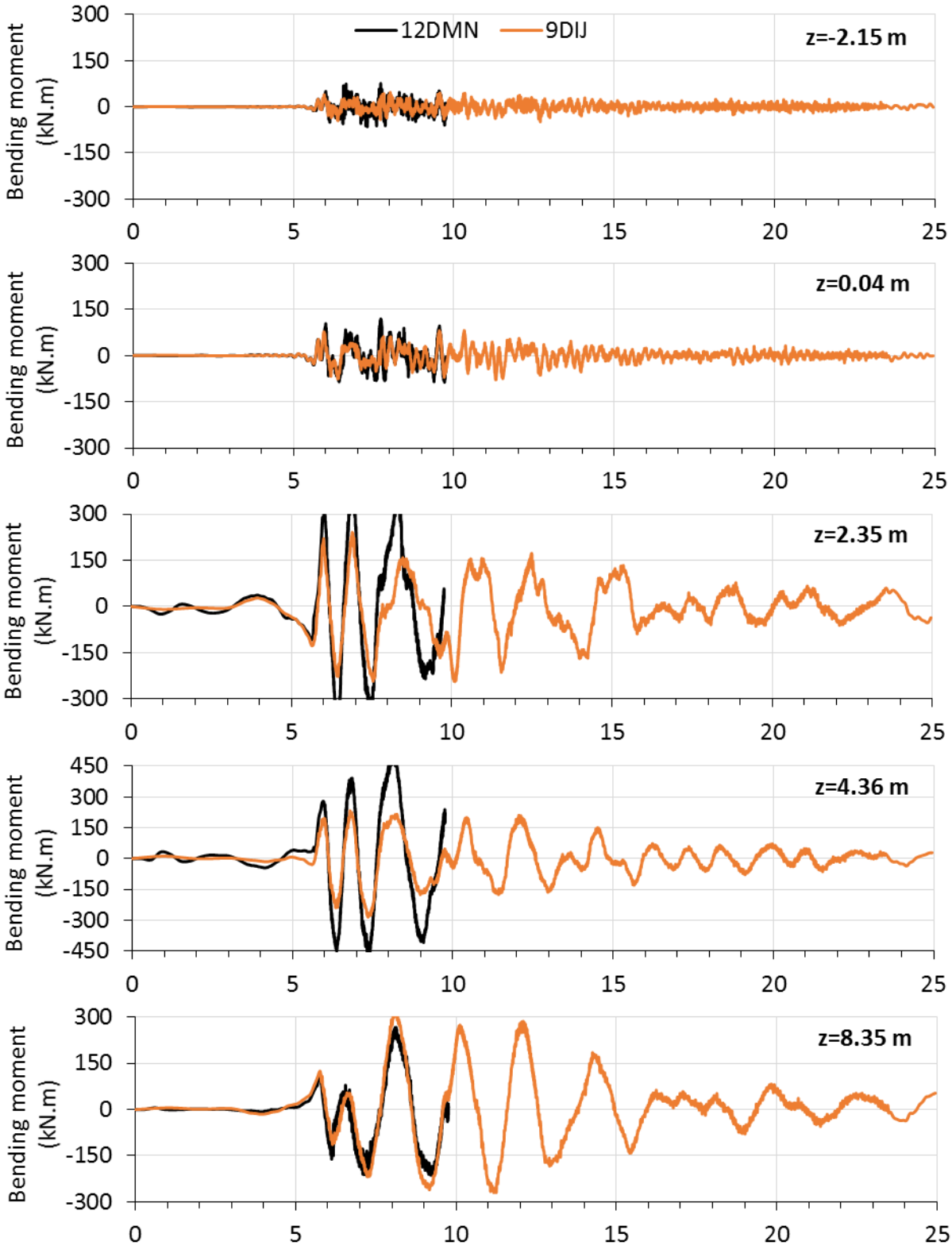

Figure 4.26 Bending moments predicted by DYPAC for 9DIJ and 12DMN for Event 3 (z is depth from the ground surface; negative values implies above ground.)

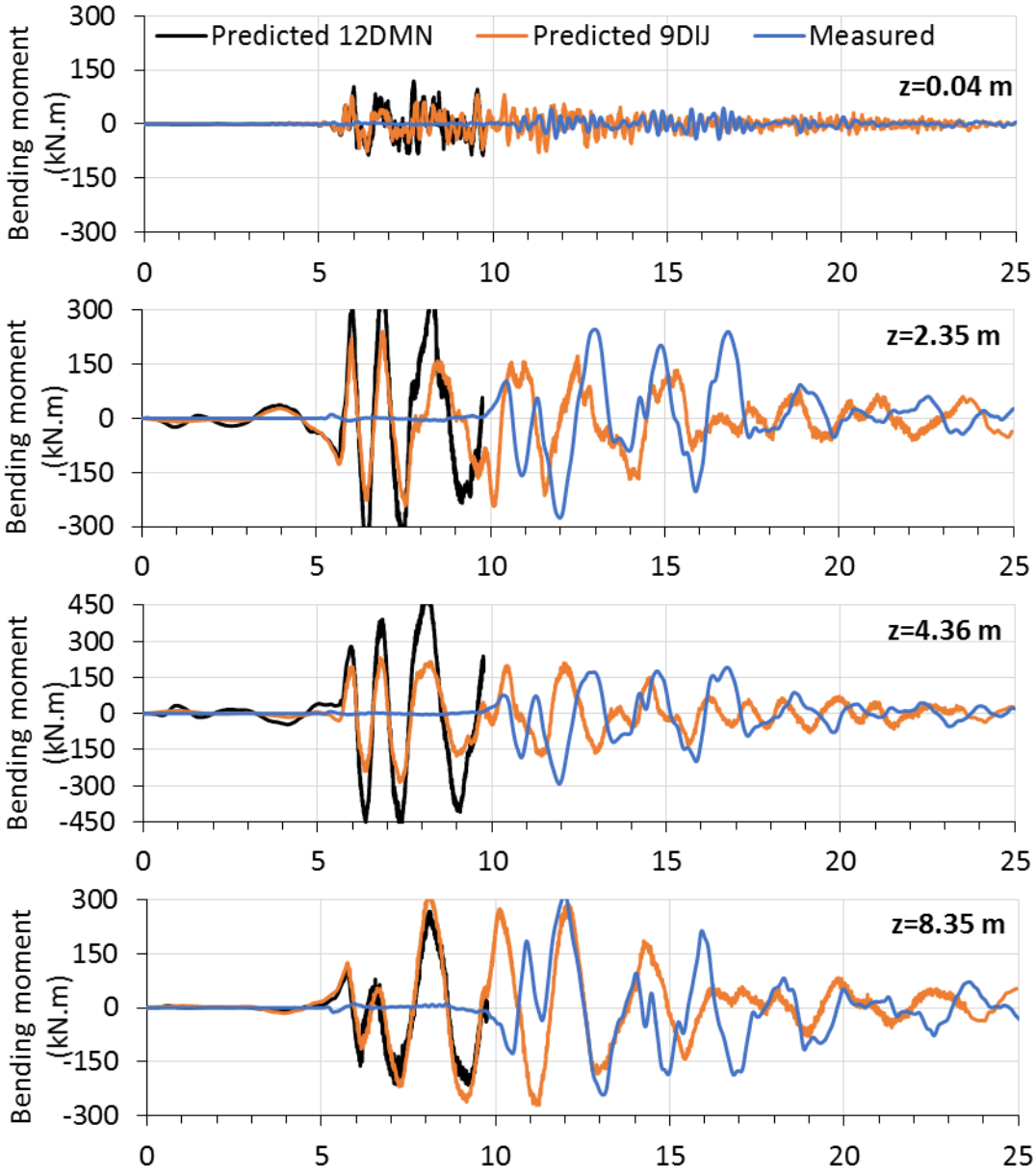

Figure 4.27 DYPAC-predicted and measured bending moment-time histories for 12DMN for Event 3 (z is depth from the ground surface)

CHAPTER 5: SUMMARY, CONCLUSIONS AND RECOMMENDATIONS FOR FUTURE WORK

5.1 Summary and Conclusions

A simple method to modify *p-y* curves was proposed to account for limited lateral extent of ground improvement. The input parameters for these curves are directly obtained from in-situ or laboratory soil tests. The CDSM improved soft clay is modeled as a stiff clay with modifications for initial soil stiffness (k) and undrained shear strength (S_u). Using the proposed modifications, the pseudo-static pile responses in CDSM improved soft clay were predicted using the LPILE computer code. The LPILE-predicted values were compared with the centrifuge test results (Liu et al., 2016). Piles modeled with linear sections reasonably predicted the responses in improved and unimproved soils for smaller static loads. The close agreement between the LPILE-predicted pile deflections (± 6%) with the measured values confirm that the proposed method for modifying the *p-y* curve is reasonable, especially when piles have not yielded.

A stand-alone computer code called DYPAC (Dynamic Piles Analysis Code) using the Beams on Non-linear Winkler Foundation (BNWF) approach was developed in this research. DYPAC analyzes the seismic response of a single pile in improved and unimproved soils. This computer code models the pile as a beam element and the non-linear soil behavior as springs and viscous dashpots using the non-linear *p-y* element developed by Boulanger et al. (1999). This non-linear *p-y* element accounts for soil yielding, gapping, radiation damping, and soil cave-in and recompression during seismic loading simulations. These *p-y* curves were modified using the approach described above to account for limited lateral extent of the ground improvement. Free-field site response analyses were performed in DEEPSOIL computer program and the soil

displacement-time histories were input to the free-field ends of the non-linear *p-y* elements. The predictions made by DYPAC are validated using centrifuge test results of Liu et al. (2016).

DYPAC predictions for pile displacements and bending moments, in general, are reasonable. The pile acceleration predictions are higher by an order of magnitude and resulted in noisy time histories compared to the measured results. The exact reasons for these discrepancies are still being investigated. The proposed method to modify *p-y* curves to characterize CDSM improved soil seems reasonable. Further validation analyses are, however, required.

5.2 Recommendations for Future Work

The present study neglects the pile damping in the analyses. However, the numerical model in Chapter 2 accounts for pile damping and DYPAC has an option to input properties related to pile damping and model that during seismic soil-pile interaction. Analyses with pile damping could improve the overall predictions and should be investigated.

The current investigation used an equivalent linear method for site response analyses to get the free-field soil displacements. It would be worthwhile to obtain these displacement-time histories using a non-linear analysis computer code such as DYSAC2 (Muraleetharan et al., 1988, 1997b).

Using the proposed modifications for *p-y* curves, the pseudo-static pile responses in CDSM improved soft clay could be predicted in GROUP (Ensoft Inc, 2016) and compared to the centrifuge test results of Taghavi and Muraleetharan (2017).

In the present computer code, the non-linear behavior of soils is modeled using Boulanger et al. (1999) *p-y* curve. A study could be conducted to investigate the effects of input

parameters to Boulanger et al. (1999) *p-y* curve. Another potential direction for future work is to model the non-linear behavior of soil using a different BNWF. Further, the effects of soil improvement and improvement zone dimensions on seismic soil-pile interactions could be investigated using the verified code and the optimum dimensions for soil improvement around a pile can be predicted for different soil properties and pile dimensions.

References

Allotey, N., and El Naggar, M. H. (2008a). Generalized dynamic Winkler model for non-linear soil–structure interaction analysis. Canadian Geotechnical Journal, 45(4), 560-573. doi:10.1139/T07-106

Allotey, N., and El Naggar, M. H. (2008b). A numerical study into lateral cyclic non-linear soil–pile response. Canadian Geotechnical Journal, 45(9), 1268-1281. doi:10.1139/T08-050

Baber, T., T., and Noori, M., N. (1985). Random Vibration of Degrading, Pinching Systems. Journal of Engineering Mechanics, 111(8), 1010-1026. doi:10.1061/(ASCE)0733-9399(1985)111:8(1010)

Bouc, R. (1967). Forced Vibration of Mechanical Systems with Hysteresis. Paper presented at the Proceedings of 4th Conference Non-linear Oscillation, Prague.

Boulanger, R. W., Curras, C. J., Kutter, B. L., Wilson, D. W., and Abghari, A. (1999). Seismic Soil-Pile-Structure Interaction Experiments and Analyses. Journal of Geotechnical and Geoenvironmental Engineering, 125(9), 750-759. doi:10.1061/(ASCE)1090-0241(1999)125:9(750)

Bray, J. D., Espinoza, R. D., and Soga, K., and Taylor, R. L. (1995). GeoFEAP—Geotechnical finite element analysis program. University of California, Berkeley, Calif.

Ensoft, Inc. (2016). "LPILE Plus Version 5.0: A Program for the Analysis of Piles and Drilled Shafts under Lateral Load," User's Manual, Austin, Texas.

Finn, L., W. D. (2005). A Study of Piles during Earthquakes: Issues of Design and Analysis. Bulletin of Earthquake Engineering, 3(2), 141. doi:10.1007/s10518-005-1241-3

Fleming, B. J., Huang, J.-W., and Sritharan, S. (2012). Seismic Behavior of Full-Scale Piles in Improved Soft Clay. Paper presented at the 37th Annual Conference on Deep Foundations Houston, Texas.

Fleming, B. J., Sritharan, S., Miller, G. A., and Muraleetharan, K. K. (2016). Full-Scale Seismic Testing of Piles in Improved and Unimproved Soft Clay. Earthquake Spectra, 32(1), 239-265. doi:10.1193/012714eqs018m

Gerolymos, N., and Gazetas, G. (2005a). Constitutive model for 1-D cyclic soil behavior applied to seismic analysis of layered deposits. Soils and Foundations, 45, 147-159. doi:10.3208/sandf.45.3_147

Gerolymos, N., and Gazetas, G. (2005b). Phenomenological model applied to inelastic response of soil-pile interaction systems. Soils and Foundations, 45(4), 119-132.

Gerolymos, N., and Gazetas, G. (2006). Development of Winkler model for static and dynamic response of caisson foundations with soil and interface non-linearities (Vol. 26).

GUO, W. D. and LEE, F. H., 2001. Load transfer approach for laterally loaded piles.

International Journal for Numerical and Analytical Methods in Geomechanics, 25(11), 1101-1129. doi:10.1002/nag.169

Hashash, Y. M. A., Musgrove, M. I., Harmon, J. A., Groholski, D., Phillips, C. A., and Park, D. (2016). DEEPSOIL V6.1, User Manual. Retrieved from Urbana, IL.

Hilber, H. M., Hughes, T. J. R., and Taylor, R. L. (1977). Improved numerical dissipation for time integration algorithms in structural dynamics. Earthquake Engineering & Structural Dynamics, 5(3), 283-292. doi:10.1002/eqe.4290050306

Kirupakaran, K., Cerato, A., Liu, C., Miller, G., Muraleetharan, K., D Pinilla, J., M Thompson, Z. (2010). Simulation of a Centrifuge Model Test of Pile Foundations in CDSM Improved Soft Clays.

Liu, C., Soltani, H., Muraleetharan, K. K., Cerato, A. B., Miller, G. A., and Sritharan, S. (2016). Cyclic and seismic response of single piles in improved and unimproved soft clays. Acta Geotechnica, 11(6), 1431-1444. doi:10.1007/s11440-016-0504-2

Loh, C.-H., and Chung, S.-T. (1993). A three-stage identification approach for hysteretic systems. Earthquake Engineering & Structural Dynamics, 22(2), 129-150. doi:10.1002/eqe.4290220204

Matlock, H. (1970) "Correlations for design of laterally loaded piles in soft clay," Proceeding of 2nd Annual Offshore Technology Conference, Vol. 1, pp. 557-594.

Mazzoni, S., McKenna, F., Scott, M. H., and Fenves, G. L. (2006). OpenSees command language manual.

Muraleetharan, K.K., Mish, K.D., Yogachandran, C., and Arulanandan, K. (1988). "DYSAC2 (Version 1.0): Dynamic soil analysis code for 2-dimensional problems", Computer Code, Department of Civil Engineering, University of California, Davis, California.

Muraleetharan, K. K., Mish, K. D., and Arulanandan, K. (1994). A fully coupled non-linear dynamic analysis procedure and its verification using centrifuge test results. International Journal for Numerical and Analytical Methods in Geomechanics, 18(5), 305-325. doi:10.1002/nag.1610180503

Muraleetharan, K.K., Mish, K.D., Yogachandran, C., and Arulanandan, K. (1997b). "User's manual for DYSAC2 (Version 7.0): Dynamic soil analysis code for 2-dimensional problems", Technical Report, School of Civil Engineering and Environmental Science, University of Oklahoma, Norman, Oklahoma.

Muraleetharan, K. K., Ravichandran, N., and Taylor, L. M. (2003). TeraDysac: TeraScale dynamic soil analysis code. Computer Code. School of Civil Engineering and Environmental Science. University of Oklahoma, Norman, Oklahoma.

Ohtsuka, S., Yamada, E., and Matsuo, M. (1996). "Bearing capacity analysis of reinforced ground,"

Proc. of Int. Symp. on Earth Reinforcement. Fukuoda, Vol. 1. pp. 647-652.

Ordonez, Gustavo A. (2012). SHAKE2000 - A computer program for 1-D Analysis of GEotechnical Earthquake Engineering Problems. GeoMotions, LLC; Lacey, Washington, USA.

Pelliciari, M., Marano, G. C., Cuoghi, T., Briseghella, B., Lavorato, D., and Tarantino, A. M. (2018). Parameter identification of degrading and pinched hysteretic systems using a modified Bouc–Wen model. Structure and Infrastructure Engineering, 14(12), 1573-1585. doi:10.1080/15732479.2018.1469652

‘‘Recommended practice for planning, designing and constructing fixed offshore platforms.’’ (1987). *17th Ed., API Recommended Pract. 2A (RP 2A),* American Petroleum Institute.

Reese, L., Cox, W., and Koop, F. (1974). Analysis of Laterally Loaded Piles in Sand. Paper presented at the Offshore Technology Conference, Houston, Texas.

Reese, L. C. and Cox, W. R. (1975). “Field testing and analysis of laterally loaded piles in stiff clay,” 7th Annual Offshore Technology Conference, Huston, Texas, pp. 672-690.

Reese, L. C., and Welch, R. C. (1975). “Lateral loading of deep foundations in stiff clay,” Journal of Geotechnical Engineering Division, Vol. 101, No. 7, pp. 633 - 649.

Sengupta and Li, (2013). “Modified Bouc–Wen model for hysteresis behavior of RC beam–column joints with limited transverse reinforcement,” Engineering Structures, Vol. 46, pp. 392-406.

Soltani, H. (2016). Development of soil-pile interaction models in improved soils using centrifuge test data and system identification methods. (Ph.D.), University of Oklahoma.

Soltani, H., and Muraleetharan, K. K., (2018). Predicting Seismic Response of a Single Pile in Cement-Treated Soft Clay Using a Bouc-Wen Type Model. Paper presented at the IFCEE 2018 : Installation, Testing, and Analysis of Deep Foundations.

Soneji, B., and Jangid, R. (2008). Influence of soil–structure interaction on the response of seismically isolated cable-stayed bridge (Vol. 28).

Sritharan, S. and Huang, J., 2010. Characterizing Lateral Load Behavior of a Pile in Improved Soils Surrounded by Soft Clay using the Winkler Analysis Concept. In Proceedings of the Annual Geo-congress of the Geo-Institute of ASCE: Advances in Analysis & Design. West Palm Beach, Florida, pp. 1622-1632.

Taghavi, A., and Muraleetharan, K. K., (2012). Seismic Response of CDSM Improved Soft Clay Sites Supporting Single Piles. Paper presented at the GeoCongress 2012 : State of the Art and Practice in Geotechnical Engineering.

Taghavi, A., Muraleetharan, K. K., and Miller, G. A. (2017). Non-linear seismic behavior of pile groups in cement-improved soft clay. Soil Dynamics and Earthquake Engineering, 99, 189-202. doi:10.1016/j.soildyn.2017.05.019

Taghavi, A., and Muraleetharan, K. K. (2017). Analysis of Laterally Loaded Pile Groups in Improved Soft Clay. International Journal of Geomechanics, 17(4).

Thompson, Z. M. (2011). Stress-strain behavior of unimproved and cement-improved soft clays. (M.S.), University of Oklahoma. Available from http://worldcat.org/z-wcorg/database.

Wen, Y.-K. (1976). Method for Random Vibration of Hysteretic Systems. Journal of the Engineering Mechanics, 102(2), 249-263.